

Submarine Lava Flow Emplacement at the East Pacific Rise 9° 50'N: Implications for Uppermost Ocean Crust Stratigraphy and Hydrothermal Fluid Circulation

Daniel Fornari¹, Maurice Tivey¹, Hans Schouten¹, Michael Perfit²,
Dana Yoerger¹⁺, Al Bradley¹⁺, Margo Edwards³, Rachel Haymon⁴,
Daniel Scheirer⁵, Karen Von Damm⁶, Timothy Shank^{1#}, Adam Soule¹

Meter scale seafloor topography and sidescan backscatter imagery of volcanic terrain along the axis of the fast-spreading northern East Pacific Rise (EPR) near 9° 50'N, coupled with visual and photographic observations provide data that constrain spatial relationships between hydrothermal vents and primary volcanic features and processes along the EPR axis. High-temperature ($\geq 350^{\circ}\text{C}$) hydrothermal vents are present in several areas within the EPR axial trough where recent eruptions have been focused and where drainback of lava into the primary eruptive fissure occurred. Chaotic collapse crusts and draped sheet lava surfaces along the margin of eruptive fissures typify sites where drainback primarily occurred. These areas are also coincident with $\sim 10\text{--}30$ m-wide channels that serve to transport lava across the crestal plateau. Regions of diffuse hydrothermal flow at low temperatures ($< 35^{\circ}\text{C}$) and vent animal communities are concentrated along the primary eruptive fissure that fed the 1991 eruption at the 9° 50'N EPR area. The relationship between seafloor eruption processes and hydrothermal vent locations within the EPR axial trough is linked to the formation of high permeability zones created by: focusing of eruptions along discrete portions of fissures; volcanic episodicity during eruptive phases lasting hours to days; and drainback of lava into the primary fissure at these same locations during waning stages of seafloor eruptions.

¹Woods Hole Oceanographic Institution, Geology & Geophysics Department, Woods Hole, Massachusetts

¹⁺Woods Hole Oceanographic Institution, Applied Ocean Physics and Engineering Department, Woods Hole, Massachusetts

^{1#}Woods Hole Oceanographic Institution, Biology Department, Woods Hole, Massachusetts

The Thermal Structure of the Ocean Crust and the Dynamics of Hydrothermal Circulation

Geophysical Monograph 148

Copyright 2004 by the American Geophysical Union

10.1029/148GM08

²University of Florida, Department of Geological Sciences, Gainesville, Florida³University of Hawaii, Hawaii Institute of Geophysics and Planetology, School of Ocean and Earth Science and Technology, Honolulu, Hawaii

⁴University of California–Santa Barbara, Department of Geological Sciences and Marine Sciences Institute, Santa Barbara, California

⁵Brown University, Department of Geological Sciences, Providence, Rhode Island, now at: U.S. Geological Survey, Menlo Park, California

⁶University of New Hampshire, Complex Systems Research Center, EOS, Durham, New Hampshire

1. INTRODUCTION

The injection of magma, eruption of lava and tectonic stresses associated with seafloor spreading at the global MOR crest profoundly impact the structure and permeability of the upper ocean crust, and hence the location and style of hydrothermal venting in different spreading environments [e.g., *Von Damm*, 1990, 1995, 2004; *Haymon et al.*, 1991; *Fornari and Embley*, 1995; *Humphris*, 1995; *Alt*, 1995; *Hannington et al.*, 1995; *Wright et al.*, 1995b, 1998, 2002; *Haymon*, 1996; *Wilcock*, 1998; *Perfit and Chadwick*, 1998; *Carbotte and Scheirer*, 2003]. To a first order, heat from magma bodies and intrusions that reach various levels in the ocean crust drive deep and shallow hydrothermal circulation systems that distribute fluids through the crust, to the seafloor, and into the hydrosphere. Vertical to near-vertical fractures, millimeters to ~ 1 m wide, created by tectonic or magmatic processes serve as pathways within crustal rocks [*Wright et al.*, 1995b, 1998]. Interflow and intraflow permeability within volcanic sequences of the upper oceanic crust further augments and complicates the geometry of fluid flow [e.g. *Fornari et al.*, 1998a]. Volcanic and hydrothermal processes at the mid-ocean ridge (MOR) crest are considered closely linked, although the temporal and spatial relationships between them have been difficult to determine.

The complex nature of submarine lava emplacement processes, the difficulty in directly observing or measuring deep seafloor eruptions, and the causal relationships between volcanic and tectonic processes at the MOR crest have been vexing problems—all of which require innovative technical and conceptual solutions [e.g., *Perfit and Chadwick*, 1998; *Fox et al.*, 2001]. Until recently, the resolution of seafloor imaging sonars has been too coarse to resolve fine-scale (~ 1 – 2 m) features required to make accurate spatial correlations between volcanic and hydrothermal features. Only within the past 15 years has sufficiently high-resolution sidescan sonar imaging of the seafloor revealed the plan-view arrangement of individual MOR lava flows and their relationship to tectonic and other features along the ridge crest [e.g., *Haymon et al.*, 1991; *Embley and Chadwick*, 1994; *Embley et al.*, 1995; *Fornari et al.*, 1998a; *Delaney et al.*, 1998; *Bohnenstiehl and Kleinrock*, 1999, 2000; *Sinton et al.*, 2002; *White et al.*, 2002]. The advent of high frequency scanning altimetric sonars and near-bottom multibeam sonars, and their application to producing meter to sub-meter scale bathymetry of small areas of seafloor, has revolutionized the study of seafloor morphology. These data can also provide clues about the structural and morphological responses of the ridge axis to magmatic and tectonic processes occurring over short (e.g., decadal) time periods [e.g., *Yoerger et al.*, 1996, 2002; *Chadwick et al.*, 2001; *Carbotte et al.*, 2003;

Schouten et al., 2001, 2002; *Embley et al.*, 2002, *Johnson et al.*, 2002; *Shank et al.*, 2002; *Fornari et al.*, 2003a; *Cormier et al.*, 2003].

A key to understanding complex relationships between volcanic and hydrothermal features at the MOR crest in both space and time is accurate, quantitative mapping of seafloor topography and the ability to repeat the surveys with well-constrained navigation. Such studies should include identifying spatial relationships between hydrothermal vents, and the axial trough or graben walls, primary eruptive fissures and zones of lava drain back, and various lava flow morphologies. Studies of subaerial lava flow morphology, timing of eruptions, flow transitions, channelized flows and textural characterization of flows imaged by land-based radar systems have provided significant insight into eruption history, dynamics and related processes on Iceland and Hawaii [e.g., *Heliker et al.* 1998; *Cashman et al.*, 1999; *Wylie et al.*, 1999; *Crown and Balogna*, 1999; *Polacci et al.*, 1999; *Byrnes and Crown*, 2001, 2003; *Parfitt and Wilson*, 1994; *Parfitt et al.*, 2002; *Soule et al.*, 2004]. Similar types of studies are critical to understanding submarine volcanic eruptions at the MOR and their relationships to hydrothermal processes [e.g., *Gregg et al.*, 1996, 2000, *Fornari et al.*, 1998a; *Embley et al.*, 1999; *Chadwick et al.*, 1999; 2001; *Sakimoto and Gregg*, 2001; *Umino et al.*, 2002; *Perfit et al.*, 2003; *Chadwick*, 2003; *Embley and Baker*, 2003]. The extreme difficulties associated with observing active submarine eruption processes also require development of conceptual, physical volcanological models based on submarine volcanic morphologies (e.g., lava pillars, flow structures and transitions) and the geochemistry and petrology of submarine lavas [e.g., *Perfit and Chadwick*, 1998; *Sinton et al.*, 2002; *Gregg and Sakimoto*, 2001; *Perfit et al.*, 2003; *Chadwick et al.*, 2003].

In this study, we explore the relationships between primary volcanic processes at a fast-spreading MOR axis and the features developed during seafloor eruptions, and their impact on hydrothermal fluid flow in the upper ocean crust. We use recently collected 120 kHz sidescan sonar imagery [e.g., *Scheirer et al.*, 2000], and micro-bathymetry data derived from a mechanically scanned altimeter on the autonomous vehicle *ABE* [*Yoerger et al.*, 1996; 2002] to map the EPR axis and summit plateau near $9^{\circ} 50' N$ (Plate 1). Near-bottom magnetic data are also analyzed to infer local regions of focused hydrothermal fluid flow, similar to observations at the Main Endeavour vent field on the Juan de Fuca Ridge [*Tivey and Johnson*, 2002]. These data sets are interpreted in conjunction with photographic and visual documentation of numerous hydrothermal vents within the axial summit trough (AST) of the EPR [*Haymon et al.*, 1991; *Fornari et al.*, 1998a] to deduce the subsurface volcanic stratigraphy and to conceptually model the complex geometry of hydrother-

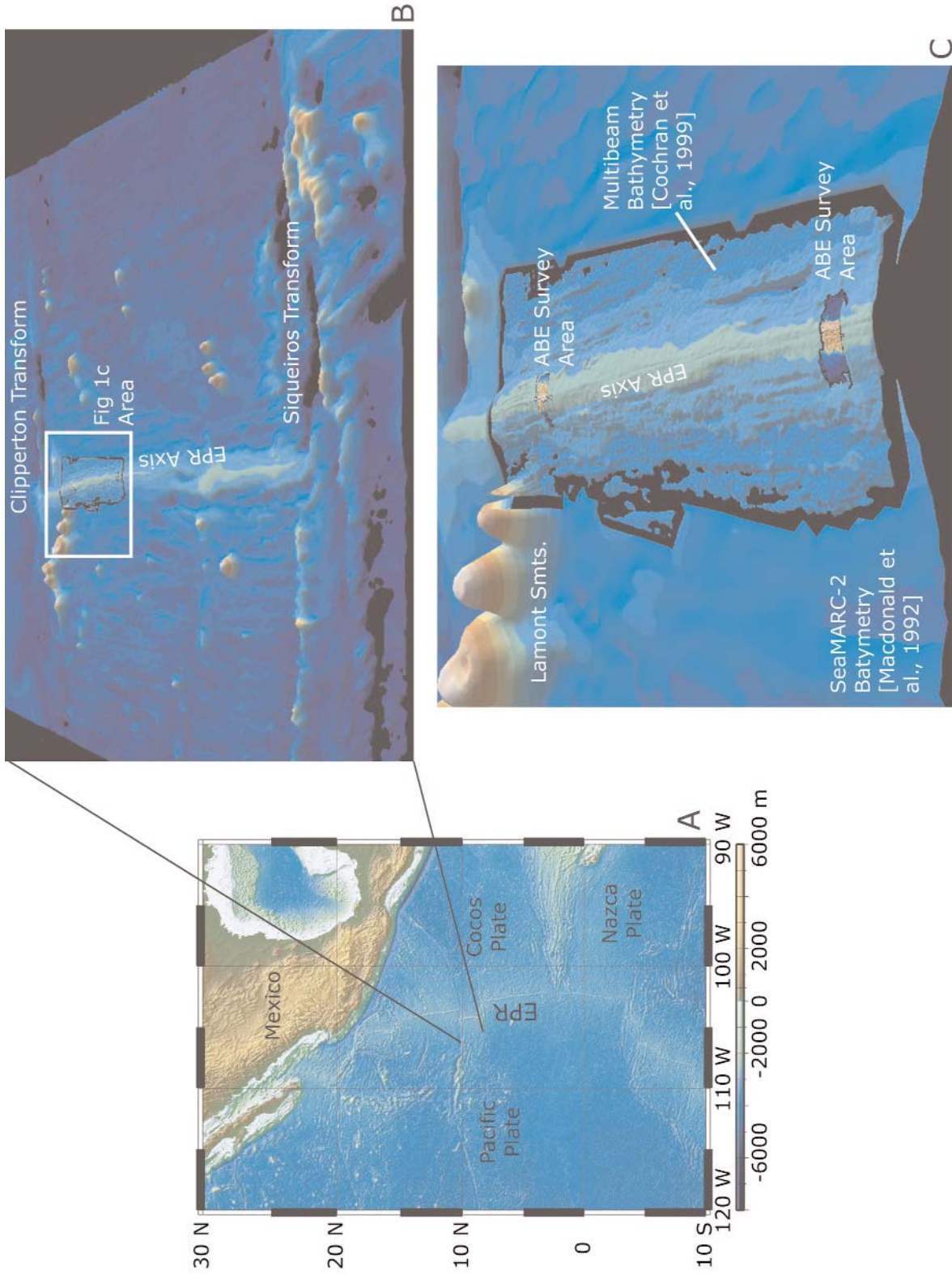


Plate 1. A) Regional location map of the eastern Pacific showing EPR axis and plate boundaries. B) Location map of the EPR based on SeaMARC2 bathymetry [Macdonald *et al.*, 1992] and multibeam sonar data [Cochran *et al.*, 1999] between the Clipperton and Siqueiros transforms. Gridded data (300 m) were visualized with Fledermaus software (<http://www.ivs.unb.ca/Products/fledermaus>). C) Close-up view of area shown by white box in 1B, with multibeam data gridded at 80 m imbedded within the coarser resolution SeaMARC2 bathymetry. Multibeam data show details of axial and off axis terrain along the EPR between 9° 25' N and 9° 55' N. Inset multi-color areas are sites of ABE micro-bathymetry surveys near 9° 28' N and 9° 50' N.

mal fluid flow in the shallow ocean crust [*German and Von Damm, 2004*]. A selection of time-series temperature records from the main high-temperature hydrothermal vents in the 9° 50' N area further substantiates the complexity in shallow subsurface flow between adjacent vents, biological communities living in diffuse flow surrounding the black-smokers, and other vents present in the axial trough between 9° 49'–51' N. These data, together with the data presented in *Von Damm [2004, this volume]*, suggest a shallow heat source. The quantitative bathymetric and sidescan sonar maps, along with observational data, provide key evidence for linking the spatial distribution of high- and low-temperature hydrothermal vents within the axial trough in the 9° 50' N area to primary volcanic features, especially the eruptive fissure that fed the recent lava flows.

2. THE EAST PACIFIC RISE 8°–11°N: BACKGROUND

The EPR between 8°N and 11°N is spreading at a full rate of 11 cm/yr [*Carbotte and Macdonald, 1992*]. The area includes: a complete 1st order ridge segment and its two bounding transform faults (right-stepping Clipperton and left-stepping Siqueiros) (Plate 1); two 2nd order segments separated by an overlapping spreading center (OSC) at 9° 03' N; and, multiple finer-scale segments, including 3rd order volcanic segments with boundaries detectable in multibeam bathymetry data, and 4th order segments bounded by smaller, more transient ridge axis discontinuities that are below the resolution of current multibeam sonar systems [e.g., *Haymon et al., 1991; Macdonald et al., 1984; Scheirer and Macdonald, 1993; White et al., 2002*].

Existing regional magnetic, gravity and multibeam/Sea MARC II sonar surveys have completely imaged the ridge flanks beyond 100 km from the axis on both sides [*Macdonald et al., 1992; Carbotte and Macdonald, 1992; Cochran, 1999; Pockalny et al., 1997; Schouten et al., 1999*] (Plate 1). Analysis of these data sets has revealed the structure, duration, migration, and temporal behavior of segment boundaries, changes in spreading directions and corresponding changes in ridge segment configuration over the past two million years, the development of faults and abyssal hills, and the distribution of off-axis volcanoes. Near-bottom acoustic and photographic surveys of the ridge crest at 9°–10° N have shown the more recent and fine-scale volcanic segmentation of the ridge crest and its relationship to the distribution of ridge crest hydrothermal and volcanic features [e.g., *Haymon et al., 1991; Fornari et al., 1998a; Kurras et al., 2000; Von Damm, 2000, 2004; Von Damm et al., 1995; Engels et al., 2003; White et al., 2002*] (Plate 2). Fine-scale bathymetric mapping available for this area from the late 1980s to 2001 consisted solely of single, near-bottom altimeter pro-

files acquired during Alvin dives or Argo II lowerings. Improvements in sonar and vehicle technology over the last ~5 years have allowed very detailed (~1–5 m resolution) bathymetric surveys to be carried out along the axis of the MOR [*Kurras et al., 2000; Chadwick et al., 2001; Johnson et al., 2002; Jakuba et al., 2002; Fornari et al., 2003a; White et al., 2000*] (Plate 3).

The only well-established magmatic events known to have affected this segment of the EPR during the past decade occurred in a region centered near 9° 50' N in ~ March, 1991 and again late in 1991 or early 1992 [*Haymon et al. 1993; Rubin et al., 1994*]. Various studies have described the hydrothermal, geochemical and biological ramifications of the 1991–92 events [*Haymon et al., 1993; Lutz et al., 1994; Perfit et al., 1994; Fornari, et al., 1998b; Shank et al., 1998; Von Damm, 1995; Von Damm, 2000, 2004; Von Damm and Lilley, 2004*]. *Smith et al. [2001]* document the volcanological and associated hydrothermal effects of the eruption on the small overlapping spreading center (OSC) at 9° 37' N. A previous EPR axial eruption is thought to have taken place during the 1987–1989 time frame in the 9° 17' N region based on freshness of lava flows mapped using Argo I, the high temperature and vapor phase characteristics of F vent (>390°C) in 1991 and its evolution to a hydrothermal brine vent by 1994 [*Haymon et al., 1991; Von Damm et al., 1997; Fornari et al., 1998a*]. In addition, lack of an AST in the ~9° 14' N to ~9° 20' N region, and the presence of extensive lava lakes and large collapse features along the axis suggest that a relatively large volume lava flow had recently resurfaced this portion of the EPR axis, probably not more than a few years prior to the November 1989 Argo II survey [*Haymon et al., 1991; Fornari et al., 1998a*].

Multi-channel seismic and expanding spread profile data have allowed for robust determinations of seismic structure [*Vera and Diebold, 1994; Toomey et al. 1994*], magma chamber depth [*Detrick et al., 1987; Herron et al., 1980; Kent et al., 1993a,b*], melt lens width, thickness, and crystallinity [*Kent et al., 1990; Singh et al., 1998*], and layer 2A thickness [*Christeson et al., 1996; Harding et al., 1993*] along major portions of the EPR in the study area. Active source seismic refraction experiments to on-bottom receivers have led to two- and three-dimensional seismic velocity models at a variety of scales for many portions of the ridge segment [e.g., *Bazin et al., 1998; Begnaud et al., 1997; Dunn and Toomey, 1997; Tian et al., 2000; Toomey et al., 1990; Toomey et al., 1994; van Avendonk et al., 1998, 2001*]. Seafloor compliance measurements have also provided constraints on shear wave velocity structure and the distribution of melt in the lower crust [*Crawford and Webb, 2002; Crawford et al., 1999*], including substantiation of *Garmany's [1989]* observation of off-axis lower crustal melt reservoirs.

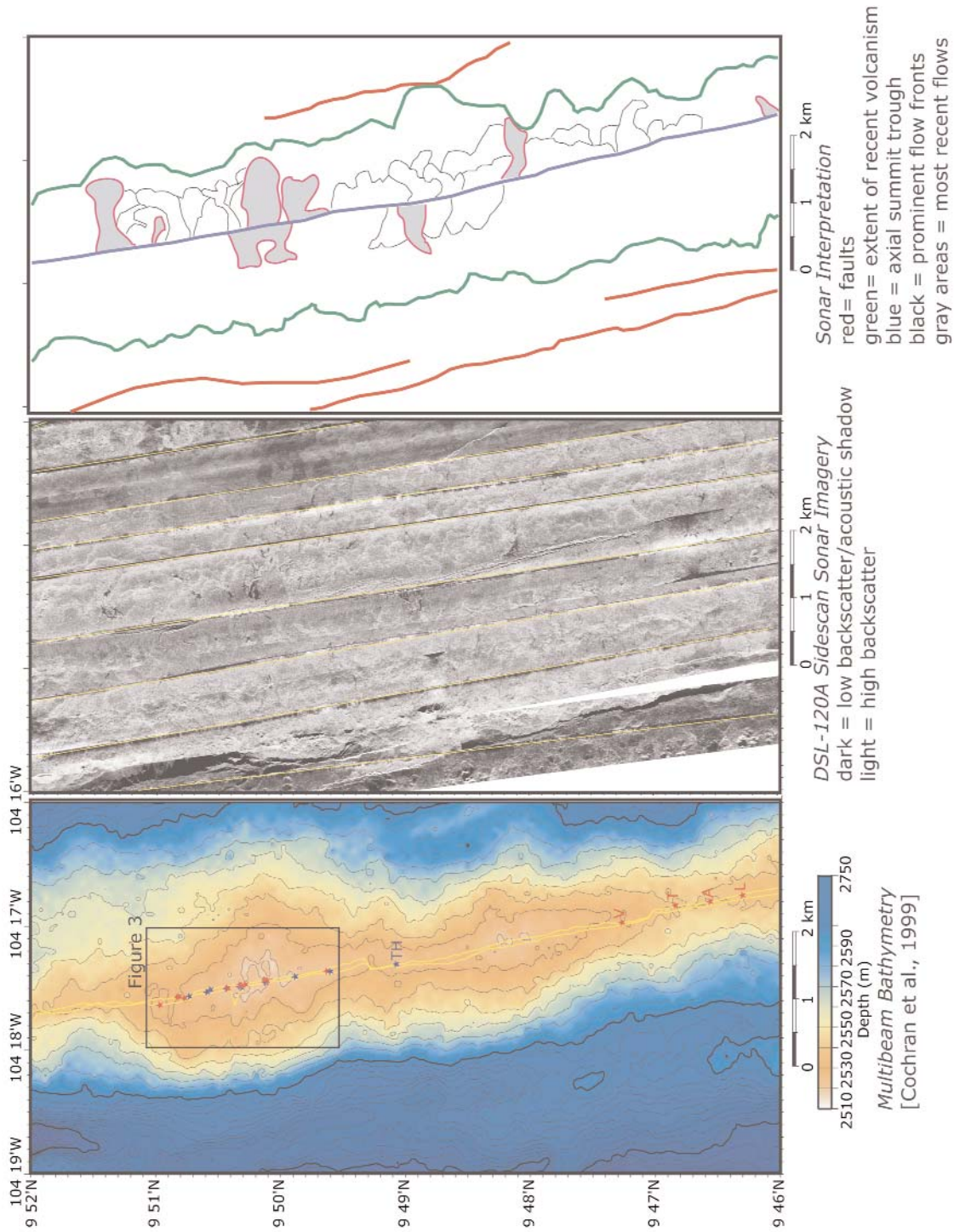


Plate 2. Left- Multibeam bathymetry showing locations of 14 high temperature hydrothermal vents (red stars) and low temperature biological communities (blue stars) along the EPR axis from 9° 46' N to 9° 51' N. Middle- DSL-120A sidescan sonar imagery for the area shown in left panel. Yellow lines show vehicle nadir. White and light gray is high backscatter, dark gray or black is low backscatter or acoustic shadow. Right- interpretative map showing faults (red lines), area encompassing most recent flows (purple lines bounding area), axial summit trough (AST) trace (blue line), scalloped flow fronts and edges (fine black lines) and most recent flows (purple lines bounding gray areas). The characteristic, shingled backscatter pattern of surficial lava flows on the EPR crest indicate a sustained eruption source within the AST (blue line) for an extensive period of time (thousands of years). The convex outward lobate flow fronts create a shingled pattern of flow lobes that trend away from the AST.

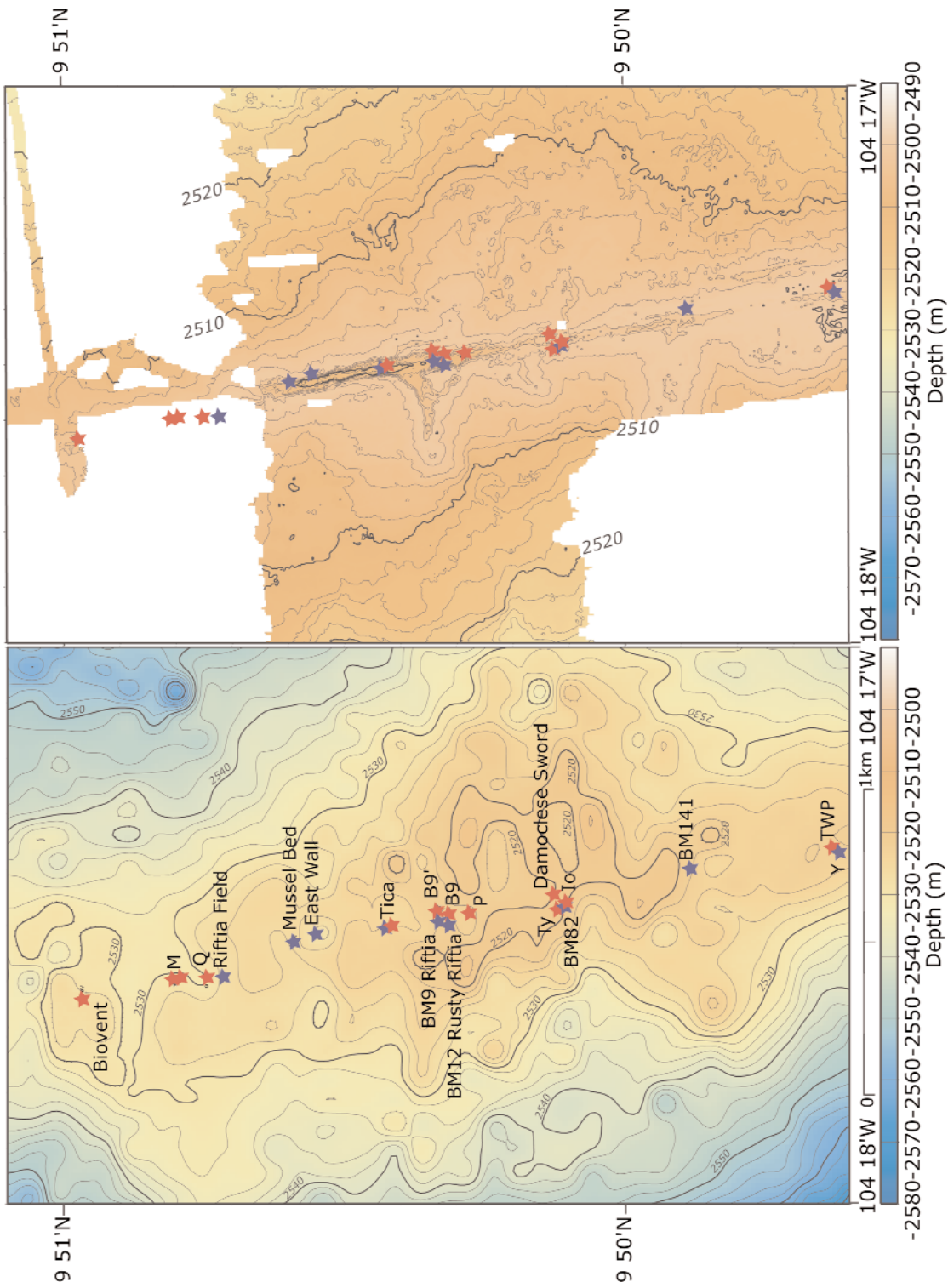


Plate 3. Left- multibeam sonar data (80 m grid, [Cochran *et al.*, 1999]) showing location of all high- (red labels) and low-temperature (blue labels) hydrothermal vents along the EPR axis between 9° 46'–51' N. Right- Detailed 2 m contours based on *ABE* 675 kHz scanning altimetric sonar surveys. Complete coverage of *ABE* micro-bathymetry data over the study area was gridded at 5 m horizontal and 1 m vertical resolution. Vent locations same as on left map. The ~20 m depth difference between the two data sets is attributed to the coarser vertical resolution of multibeam (~10–15 m) and slight differences in assumed velocities and ray paths for the multibeam data, as well as the *ABE* data being much higher frequency altimetric data added to vehicle pressure depth. The *ABE* data are considered much superior and more representative of the correct absolute depth.

3. HAWAIIAN FISSURE ERUPTIONS AND MID-OCEAN RIDGE SUBMARINE VOLCANIC FEATURES

In order to provide a volcanological context for the seafloor observations, we present brief background information on Hawaiian eruptive fissures and lava flows and compare and contrast them to MOR submarine lava eruptions and flow characteristics. Many features of submarine volcanic landforms and lava flows have analogs in their subaerial counterparts. Here we examine some features common to both environments and discuss how those features may be related. Fissure eruptions on basaltic shield volcanoes like Kilauea in Hawaii commonly initiate with eruptive activity at a point source that migrates along the length of a fissure, until it all is erupting at once (Plate 4). Eruptive activity focuses quickly, sometimes within hours, to a small number of loci that may remain active for the duration of the eruption. Over most of the fissure length, lava will flow only a short distance perpendicular to the fissure (usually < 1 km). At persistent eruptive vents narrow flows are formed (length/width $\gg 10$), the length of which depends on the volume of lava erupted and length of time that the vent is active. The Maunu Ulu 1974 and Pu'u 'O'o (1983 to present) eruptions are classic examples of persistent vents forming long tube and surface fed flows that extended tens of kilometers from their source vents [Tilling *et al.*, 1987; Wolfe *et al.*, 1987, 1988]. By comparison many submarine lava flows on the EPR in the $9^{\circ} 50' N$ area (Plate 3) appear to be ~ 1 – 2 km long and with relatively smaller l/w ratios (~ 1 – 2) as compared to Kilauea flows.

As subaerial flows extend from their eruptive source they often undergo transitions in surface morphology that reflect changes in the physical properties of the lava and eruption dynamics. In subaerial lava flows, transitions in surface and flow morphology are dependent on a host of interdependent eruption and flow parameters including eruption temperature, volumetric flow rates, cooling rates, crystallization rates, and pre-existing topography. Temporal and spatial changes in these parameters result in a characteristic evolution in surface morphology from pahoehoe to 'a'a over length scales from 0.25–4 km for medium to high effusion rate eruptions [Soule *et al.*, 2004]. It is observed that the pahoehoe-to-'a'a transition is initiated within regions of focused flow (i.e. channels) at distances from the vent where lavas have cooled and crystallized sufficiently to fundamentally change the rheology of the lava and consequently the style of lava deformation [e.g. Cashman, *et al.*, 1999; Soule, *et al.*, 2004].

An analogous down-flow transition in surface morphology is observed in submarine flows from proximal sheet flows, to lobates, to pillows. This evolution, while greatly simplified, is observed along some down-flow and cross-flow transects in our existing digital seafloor imagery. In the submarine

environment, the parameters controlling surface morphology are not dependent on lava temperature and crystal content, both of which remain relatively constant due to the rapid formation of thick, insulating crusts (e.g., Gregg and Fornari, 1998). Analog wax models of submarine lava flow emplacement identify two independent parameters of flow emplacement: the time scales of cooling and advection, and the ratio of those parameters that determines the surface morphology of the flow [Fink and Griffiths 1992, Griffiths and Fink, 1992, Gregg and Fink, 1998; Sakimoto and Gregg, 2001]. Due to the large thermal gradient between molten lava and seawater, cooling rates on submarine lava flows should be similar regardless of variation in the temperature of either the erupting lava or overlying seawater. Thus, the dominant parameter determining submarine flow morphology is the timescale of lava advection. Volumetric effusion rate and pre-existing topography provide the primary controls on this advection rate [e.g. Gregg and Fink, 1998; Sakimoto and Gregg, 2001].

One of the most distinctive morphological characteristics of the sidescan sonar data in our study area (Plate 2) are the overlapping, concave outward (from the ridge axis) reflectors that comprise the fronts of lava flows erupted at the axis. The bi-lateral symmetry of the reflectors on either side of the axis indicates that the locus of eruption has been quite constant along the axial trough for thousands of years. The scalloped flow-front morphology along volcanically and hydrothermally active portions of the EPR shown in Plates 2 and 3 is analogous to areas adjacent to the rift zones of Mauna Loa and Kilauea volcanoes (Plates 4 and 5). In Hawaii, volcanic activity has been concentrated over hundreds of thousands of years [Holcomb, 1980, 1987] and has produced high aspect ratio (flow length/width) flows that inter-finger and overlap. A potential distinction between the submarine and subaerial environments is that the EPR seafloor is actively spreading, thus flow fronts that may have reached 1 km from the vent at the time of eruption are observed at 1.5 km from the vent after 10 kyr. However, the lack of faulting within ~ 2 km of the EPR axis (equivalent to ~ 40 kyr spreading distance) relative to areas farther off-axis suggests that the area around $9^{\circ} 50' N$ is repaved over a much shorter time interval; therefore, exposed flow fronts can be assumed to have formed nearly in place. The resurfacing rate for Kilauea is estimated to be of the order of ~ 1 kyr. Holcomb [1987] estimated that $\sim 70\%$ of Kilauea's surface is younger than ~ 500 yrs; $\sim 90\%$ is younger than ~ 1.1 kyr. Resurfacing is achieved primarily through tube-fed pahoehoe flows that comprise $\sim 67\%$ of the flows, while 14% consist of surface fed pahoehoe and 16% is 'a'a lava. The sonar imagery shown in Plates 2 and 5 suggest that much of the EPR axis near $9^{\circ} 50' N$ is resurfaced rapidly, probably at rates $\ll 1$ ky, because of the abundant scalloped flow fronts and lack of recent faulting of the volcanic carapace.

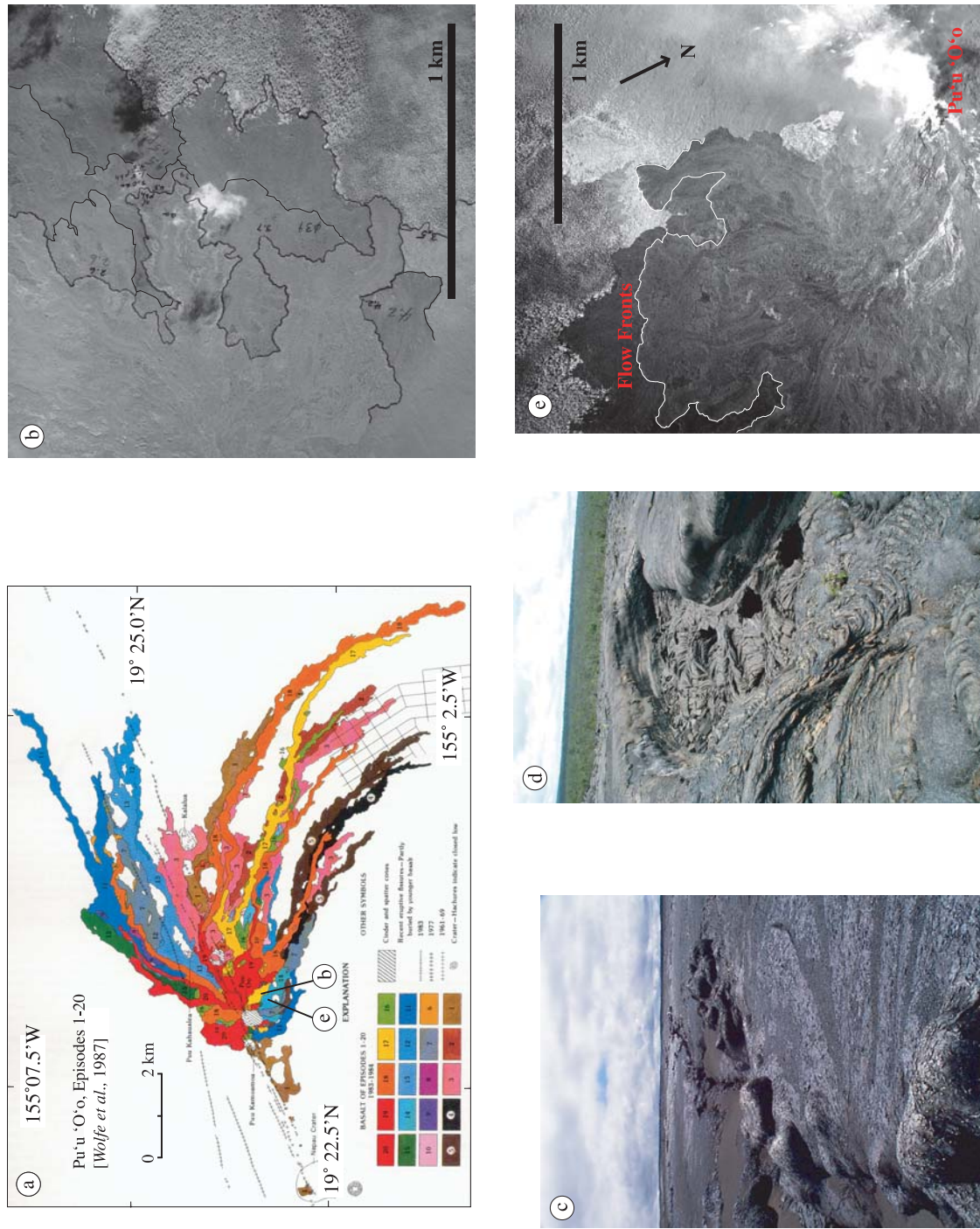


Plate 4. a) Eruptive history of Kilauea volcano, Hawaii [from Wolfe *et al.*, 1987]. b) Aerial photograph showing overlapping, scalloped flow fronts from Puu OO vent Episode 39 of the eruption (source: USGS HVO). c) Eruptive fissure along the east rift zone, showing drainback along the fissure margin. d) Lava channel on Maunu Ulu, note series of collapse pits in the floor of the channel. e) Aerial photograph showing overlapping, scalloped flow fronts from Puu OO vent Episode 40 of the eruption. The active vent is at lower right of the photograph. (source: USGS HVO).

A more appropriate analogy for individual EPR lava flows may be the overlapping of flow fronts within a single eruptive episode. For example, early episodes of the Pu'ū 'Ō'ō eruption produced multiple flow fronts over the timescale of months that look very similar to the overlapping and scalloped-edged flows observed at the EPR in the 9° 50' N area within 0–2 km from the AST (Plates 2, 4b/e, 5a). Pu'ū 'Ō'ō flows advanced primarily as 'a'a sheets; while the rheology of the flow may differ at the MOR crest, the mechanism of advance (continuous sheets fed by lava channels) is likely to be similar. In general, Pu'ū 'Ō'ō flow fronts show a scalloped margin in plan view and can contain many distinct lobes. Later flows tend to generate flow fronts that in places mirror the existing flow margin, but exploit cusps between the scallops where it is possible to advance (Plate 4b/e).

Discerning the particular lava flow related to each subaerial flow front is difficult, if not impossible, for flows that cannot be confidently traced to their origin or are not directly observed—a luxury that one does not have in the deep ocean. Subaerial eruptive episodes will often produce multiple flow lobes that are emplaced adjacent to each other [e.g., *Kilburn, 1996*]. This results in multiple, lobate flow fronts that represent a single eruptive event. Such emplacement is more common in cooling limited flows, where further advance of the flow-front is inhibited by the cooled and crystallized lava, spurring break-outs from secondary vents (“bocas”) along the existing flow path. Due to the rapid rates of cooling in the submarine environment, this process should be enhanced, and distinct flow fronts within the scalloped region may reflect approximately half as many individual eruptive episodes.

Lava drainback is a common feature near the vents of both subaerial and submarine lava flows [e.g. *Kurras et al., 2001; Engels, et al., 2003*] (Plates 4, and 6–7). Observed drainback occurrences in subaerial lavas include the cyclic filling and draining of Kilauea Iki lava lake [*Eaton et al., 1987*], Mauna Ulu [*Swanson et al. 1973; Tilling et al., 1987*], and Pu'ū 'Ō'ō vents on Kilauea's east rift zone [*Wolfe et al., 1987, 1988; Greenland et al., 1988; Barker et al., 2003*]. The process of large-scale, subaerial lava lake drainback is believed to occur after vesiculating magma in the conduit expands, causing the lava lake to fill, and then catastrophically degasses providing space for the denser, degassed lava to drain [*Barker et al., 2003*]. Smaller scale lava drainback is also observed at fissure vent eruptions where no lava lake is present. In those settings, drainback can be accomplished by the same rapid degassing mechanism, or by simply refilling the voided conduit after some volume of lava has been erupted on the surface. The timescale of drainback has been constrained for the Pu'ū 'Ō'ō lava lake by examination of geodetic and seismic records during cyclic periods of filling and draining [*Wolfe et al., 1987, 1988*]. In all cases drainback occurred rapidly, on the order of

tens of minutes. No such records exist for smaller volume eruptions, but timescales should be similar for both conduit degassing and void space drainback mechanisms. The short timescale of drainback produces some characteristic surface features that are preserved on the flow surface. On subaerial fissure eruptions, these features include draping of plastically deformed lava crusts into the evacuated vent and along fissure margins (Plate 4c/d). In some cases, this process occurs beneath a 5–25 cm thick pahoehoe crust that does not plastically deform, but breaks in to small (2–10 m²) plates which founder as the supporting lava is removed (Plate 4f). The difference between these two drainback forms results from the duration of the eruption and dynamics of lava at the vent, with the absence of a solidified upper crust signifying shorter eruptive timescales and the lack of a stagnated lava pond at the vent. Very similar lava morphologies indicating drainback are observed at the EPR within lobate, ponded and sheet flows [e.g. *Fornari et al., 1998a; Kurras et al., 2001; Engels et al., 2003*] (Plate 6).

In subaerial lava lakes and ponds, the onset of drainback coincides with violent bubbling that ejects spatter and chews through the existing lava crust. Surficial evidence of foundering crust is likely lost as drainback is generally cyclic and the floor of the lake or pond is resurfaced many times during the eruptive event. At Pu'ū 'Ō'ō, a cycle of lake-filling and -drainback occurred eleven times during a period of 50 days and then ceased. The cessation of this pattern is believed to reflect the development of a stable permeability within the conduit achieved either by the draining of blocks of crust into the upper conduit or by the formation of new sets of cracks and fluid pathways as the conduit inflated and deflated during pressurization and gas release events. With stable permeable pathways in place, volatiles can easily escape to the surface precluding the pressurization events necessary to bring lava to the surface.

Collapse and drainage features may also form where lava has not drained back into the vent, but away from the existing volcanic landform, either down-flow or laterally. Here rates of lava removal are controlled by the rheology of the slightly cooler, more crystalline lava, the geometry of fluid pathways within the molten flow interior, and the size of the aperture through which draining occurs. This process is common in subaerial flows where continued advance of the flow front is hindered by the development of a thick solidified crust (e.g. *Mattox et al. 1993; Hon et al. 1994*). In most cases, although timescales of drainaway may be similar, volumetric flux rates of drainage are considerably slower in the subaerial environment due to higher viscosities. As a result, features recording these events that are preserved on the flow surface indicate a slow sagging of the surface crust rather than foundering and rapid crustal breakup (Plate 4c/d).

At the EPR, eruptions are likely to have similar styles of eruption focusing and short-term (days to <<month?) episodicity within an eruptive phase with waxing and waning of activity. Evidence for episodicity includes multi-storied collapse features (Plate 6b, and figures in *Engels et al.*, [2003] and *Kurras et al.*, [2002]) that appear to have formed by inflation, lava withdrawal and subsequent additional inflation of the flow, with a final phase of collapse utilizing the original drain-back area, thereby exposing two prominent lava crusts within the same collapse feature. Short durations (hours to days) have also been observed for submarine eruptions monitored using hydrophone arrays in the NE Pacific, where the Axial Volcano eruption had several phases and lasted 12 days and the Coaxial eruption lasted 31 days [*Fox et al.*, 1995, 2001; *Embley et al.*, 1995; *Chadwick*, 2003].

4. DATA ACQUISITION

Sidescan sonar mapping and *ABE* surveys were carried out during a cruise on R/V Atlantis (AT7-4) in November 2000 [*Schouten et al.*, 2001; 2002] (Plate 1). *ABE* collected near-bottom magnetic data (using a 3-axis fluxgate magnetometer) and micro-bathymetry (using an Imagenex 675 kHz pencil beam altimeter) along track lines spaced ~40–60 m apart at an altitude of ~40 m above the seafloor [*Yoerger et al.*, 1996; *Tivey et al.*, 1997; 1998; *Schouten et al.*, 2001]. *ABE* surveys were navigated using long-baseline (LBL) bottom-moored transponders resulting in navigational accuracies generally better than ~5m (see *Fornari et al.* [1998a] and *Lerner et al.* [1999] for a discussion of LBL navigation techniques); RMS solutions for transponder positions for our surveys were all ≤ 1.0 m. We used the DSL-120A sonar vehicle, a 120 kHz sidescan sonar system towed at 100 m above the seafloor, capable of producing 1–2 m pixel resolution images of seafloor backscatter amplitude [e.g., *Stewart et al.*, 1994; *Scheirer et al.*, 2000]. Sidescan sonar survey lines were navigated using both LBL transponders and a layback calculation that employed sonar depth and wire out; accuracy is ~5 m.

Plate 3 shows bathymetric maps of the same area around 9° 50' N made using surface ship multibeam sonar and *ABE* near-bottom altimetry. The ~20 m depth difference between the two is attributed to the coarser vertical resolution of multibeam (~10–15m) and slight differences in assumed velocities and ray paths for the multibeam data, in addition to the *ABE* data being much higher frequency altimetric data added to vehicle pressure depth. The *ABE* data are considered much superior and more representative of the correct absolute depth. Also, we note that the trace of the AST in the sidescan data, over the 55 km long area mapped in 2001 [*Schouten et al.*, 2002] (Plate 3), is well-correlated with detailed features

mapped in 1989 using Argo II [*Haymon et al.*, 1991; *Fornari et al.*, 1998a], and in 2000 using the previous DSL-120 sonar vehicle [AHA-Nemo2 cruise, *Fornari et al.*, 2001; *White et al.*, 2002] (Plates 2 and 3). In some cases, the trough position from 1989 is offset slightly while the overall shape is consistent with sonar reflectors mapped using 2001 data, suggesting that a small (~50 to 100 m) navigational shift would correct the mismatch (D. Fornari and J. Escartin, unpublished data). Plates 3 and 5 show the trace of the AST based on analysis of the 2001 sidescan sonar data.

In 2001, we also used a prototype, digital deep sea camera system [I. Macdonald, pers. commun., 2000; *Fornari*, 2003] to image the seafloor along traverses across selected backscatter facies and volcanic contacts displayed in the sidescan imagery. Camera tows were navigated using LBL transponders with positional accuracy of ~5 m. Historical observation and photographic data from over a decade of Alvin diving in this area provided ground truth for interpretation of sonar maps and relationships between hydrothermal vent sites (Plate 2) and volcanic features within and adjacent to the AST [e.g., *Haymon et al.*, 1993; *Von Damm et al.*, 1995; 1996, 2001; *Fornari et al.*, 1998a,b; *Shank et al.*, 1998; *Engels et al.*, 2003; http://www.whoi.edu/marops/vehicles/alvin/epr_photos.html; Soule and Fornari unpublished GIS EPR photo database]. Time-series temperature data were collected using self-recording probes described in detail by *Fornari et al.* [1994, 1996, 1998a,b, 2003b]. Detailed discussion and interpretation of near-bottom magnetic data and the complete sidescan sonar data set, which cover the EPR axial region over an area centered on the AST and extending out to ~4 km on either side, between 9° 26' N to 10° N, will be presented elsewhere (*Schouten et al.*, in prep.; *Tivey et al.*, in prep.; *Fornari et al.*, in prep.).

5. EPR 9° 26'–10° N VOLCANIC HISTORY AND SEAFLOOR MORPHOLOGY

The synoptic view provided by the sidescan imagery shows the EPR axis to be dominated by the scalloped (convex outward on either side of the AST) acoustic reflectors that we interpret to be lava flow surfaces and flow fronts (Plates 2 and 5); a finding that has been corroborated by towed camera surveys and observations from Alvin. This observation is common in the near axis terrain from 9° 55' N to 9° 27' N, extending outward from the axial trough to variable distances—usually 1–2 km—on either side of the trough. Many areas of the EPR crest in the mapped region between 9° 26' N–10° N show extensive re-paving by successive, small volume flows; these are associated with short (~100–500 m), scalloped flow-front margins consistent with eruptions originating from the

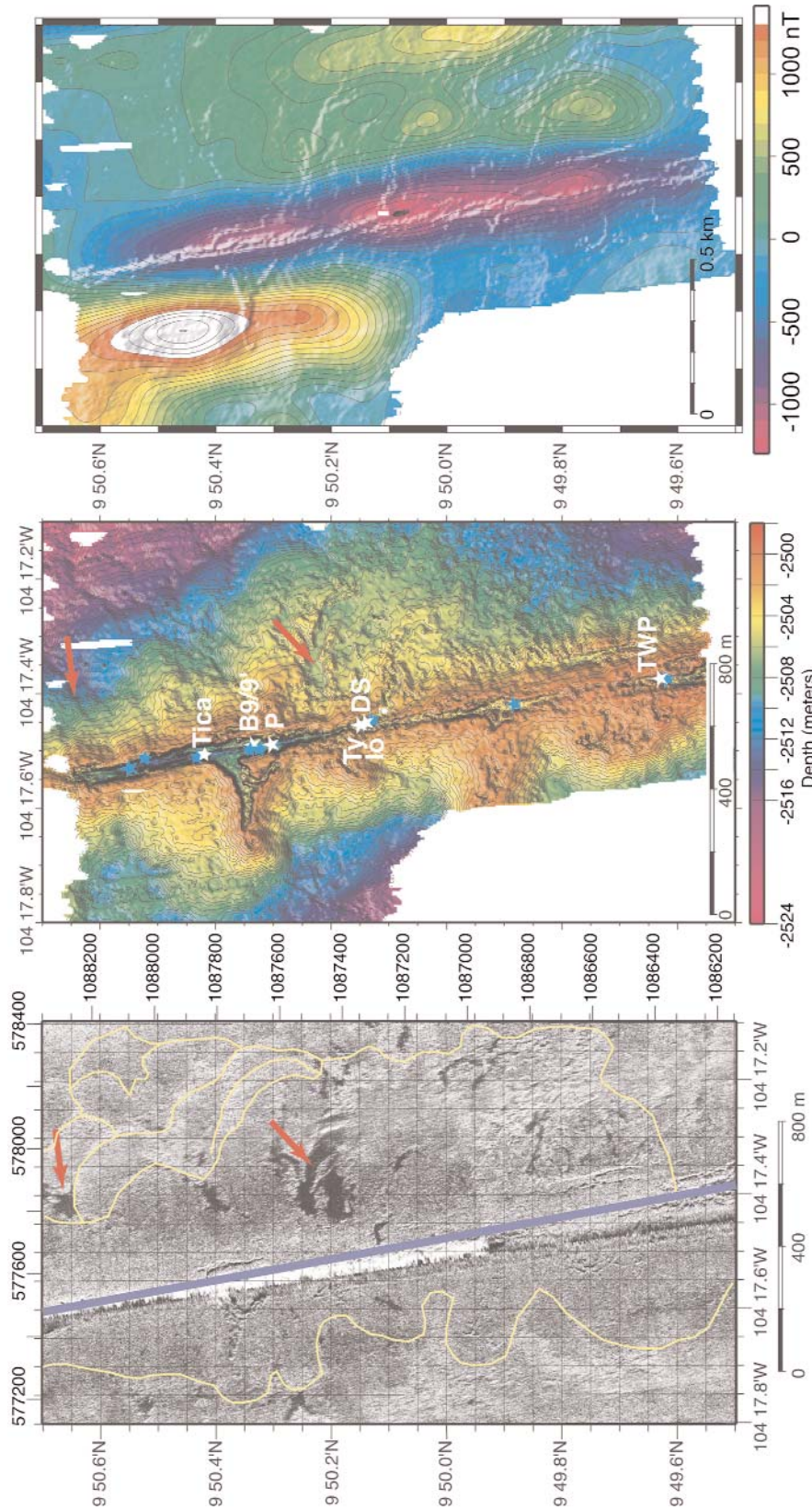


Plate 5. Left map shows a blow-up of the sidescan sonar imagery for the area around 9° 50' N, with prominent channelized sheet flows highlighted by red arrows. Middle map shows detailed micro-bathymetry [Schouten *et al.*, 2001, 2002]. High temperature vents labeled in white, low-temperature diffuse flow vents and animal communities are shown by blue stars. Red arrows point to channelized sheet flows mapped in the DSI-120A sonar data which can also be resolved by the detailed bathymetry. Right map shows reduced to pole magnetic map of the EPR AST based on ABE near-bottom magnetic data collected in 2001-02 on AI7-4 and AI7-12 cruises at same scale as other maps in this figure [Schouten *et al.*, 2001, 2002; Tivey *et al.*, 2003]. Prominent low is coincident with the axis of the axial trough suggesting very thin crust (lava) and presence of shallow dikes. Elongate closed-contour lows around northern vents (Bio9/9' and P) at 9° 50.3' N and Ty and Io vents near 9° 50.1' N suggest possible 'burn holes', that are smaller but similar to the near-bottom magnetic expression of vents imaged at JDF Main Endeavour Field [Tivey and Johnson, 2002]. Because of our 60 m line spacing, more closely spaced lines are required to properly image the smaller EPR vent systems. The prominent magnetic high just west of the AST near 9° 50.4' N is likely to be a primary depo-center for the 1991-92 eruption and is coincident with the large breakout from the AST believed to be related to extensive drain back at this location; proximal to the locus of high-temperature venting at Bio9/9' and P vents.

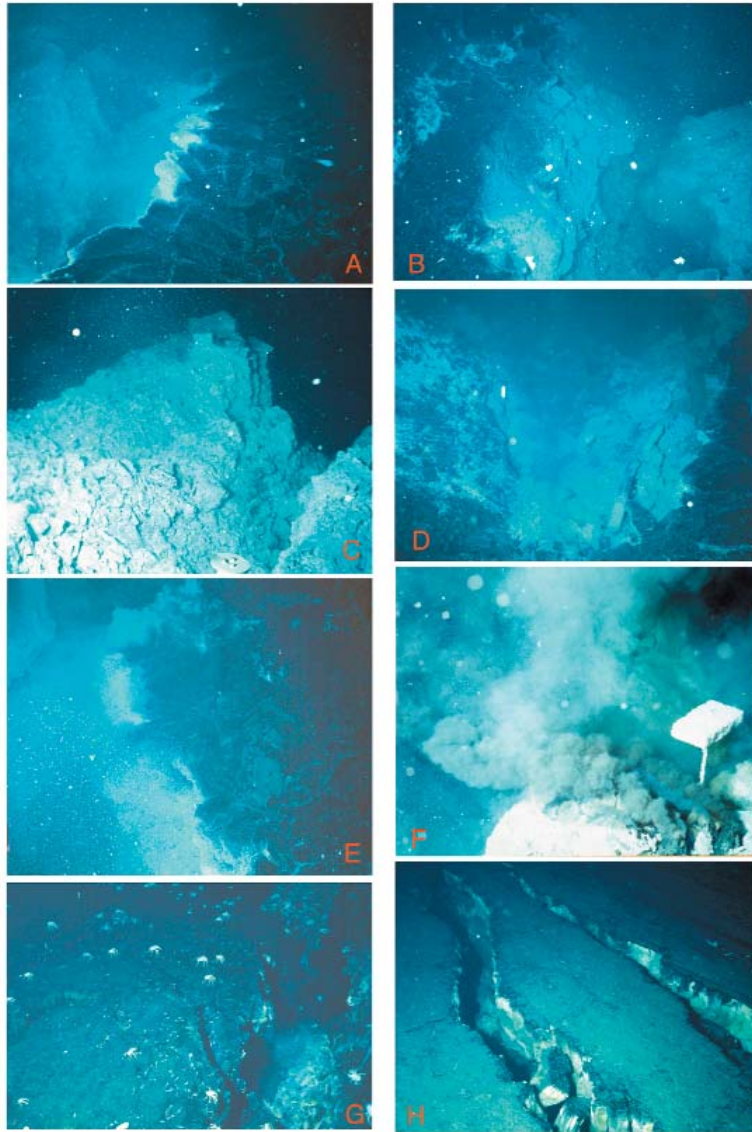


Plate 6. Morphological characteristics of the primary volcanic eruptive fissure system in the $9^{\circ}50'N$ region in April 1991 (A-F) as imaged from *Alvin*. Scale in meters across the foreground of each photograph is given in brackets at the end of each description. (A) View along the west edge of the primary eruptive fissure in the $9^{\circ}50.1'N$ region. Note platy sheet flow talus at the margin of the fissure and bacterial coating within the fissure and in cracks in the sheet flow surface [Haymon et al., 1993] [3]. (B) View inside the primary fissure in the $9^{\circ}50.0'N$ area showing bacterial covered fresh lava surfaces and inward dipping plates of sheet lava along left edge of photo [2]. (C) Bacterial mat covered tumulus in the area just north of the Bio9/9' vent area cleaved by the primary fissure [2]. (D) Talus filled axis of the primary fissure just south of area of photo in (B) where the fissure widens to $\sim 3m$ [2]. (E) Edge of the primary fissure in the $9^{\circ}49.8'N$ area showing bacteria along the wall and jumbled sheet flow talus on the floor of the AST [3]. (F) Syntactic foam marker (square at right edge of photo) covered with bacterial matter placed a few days earlier in the 'Hole to Hell' area where the Bio9/9' and P vents would later localize. Note black smoker venting issuing from bare fresh basalt at lower right corner [2]. (G) Tensional cracks in a sheet flow on the floor of the AST near $9^{\circ}30'N$ imaged in 1991 showing extensive diffuse flow and galatheid crabs and mussels (yellow/brown shells at lower right in milky water) [2]. (H) Extension of the cracks seen in photo (G) $\sim 30m$ further north where no focused low-temperature vent activity was present in 1991. The AST in the $9^{\circ}30'N$ region is $\sim 250m$ wide and shows extensive evidence of tensional cracking above recently intruded dikes, however, there is no well developed primary eruptive fissure in this area [Fornari et al., 1998a].

axis and flowing onto the upper rise flank out to ~2 km [Schouten *et al.*, 2001, 2002] (Plates 2 and 5). There are few faults within ~2 km of the AST (Plate 2), but they are more common south of the 9° 37'N OSC [Smith *et al.*, 2001]. Most faults have low relief (<~10 m), based on sonar shadow geometry and *ABE* micro-bathymetry data. Most faults parallel the 352° trend of the EPR axis in this area, but some deviate from that azimuth by as much as ~10°, and most faults show some sinuosity along their strike.

Numerous dendritic lava flow channels emanate from the AST in various sections of the ridge axis principally in the 9° 50'N, 9° 48'N, 9° 43'–45'N, 9° 37'N, and 9° 26'–29'N areas (e.g., Plates 2 and 5). These channels are similar to those identified by Cormier *et al.* [2003] at the southern EPR near 17.5°S. We confirmed with towed camera imagery in 2001 that the low-backscatter channels are flooded by smooth-surfaced sheet lava. Sidescan sonar data show that many of the channels originate at the AST rim, however some do not and they are believed to be somewhat older channels that have had their source-proximal ends paved over by more recent flows (Plate 5). Along the EPR axis between 9° 26'N and 9° 29'N, the channelized flows cover areas as great as ~5 km along strike, and coalesce away from the trough at distances of ~500 m to <1000 m [Schouten *et al.*, 2002]. Spacing between sheet flow channels can be from a few hundred meters to several kilometers.

Fields of lava mounds or ridges ~10–30 m high, some comprising coalesced volcanic constructs, are several hundred meters wide and up to ~1 km long. These features usually occur at distances of >1.5 km from the AST (White *et al.*, 2000). In some areas the mounds are concentrated at ~2–2.5 km distance from the AST (e.g., in the region between ~9° 53'–57'N, 9° 43'–47'N and 9° 31'–34'N on the east side of the axis, and at 9° 43'N, 9° 35'–36'N west of the axis). Some pillow mounds are cut by faults and fissures, while in some areas closer to the axis they are not, suggesting their construction is more recent than tectonic features they overprint [Schouten *et al.*, 2001, 2002; Kurokawa *et al.*, 2002].

Sidescan data suggest that the EPR crest has experienced four types of volcanic emplacement processes: (1) axial summit eruptions within a ~<0.5 km wide zone centered along the present trace of the AST (Plates 2 and 5); (2) off-axis transport of lava erupted within or near the AST through channelized surface flows and tubes extending to ~2 km from the axis; (3) local constructional volcanism at distances of <2 km from the axis (Plate 5); and (4) off-axis eruptions at >2 km from the AST. The predominance of lobate flows (59% of the surveyed area) throughout much of the crestal region, and common scalloped flow front morphology along much of the ridge crest suggest that individual eruptive volumes have been

small, similar to that estimated for 1991 EPR flow (~1 x 10⁶ m³, Gregg *et al.*, [1996]).

Our interpretation of lava morphology and related data sets from this ridge segment suggests that the portion of the EPR between ~9° 29'N to 9° 51'N has not experienced large-scale volcanic resurfacing in the past ~30 ka from volumetrically large eruptions that have covered broad areas of the ridge axis. Instead, the resurfacing is accomplished by frequent, small volume (<1–2 x 10⁶ m³) [Perfit and Chadwick, 1998] eruptions that do not usually extend much further than ~1–2 km from fissures within or along the AST—the predominant eruptive lineament along the axial zone. Based on sonar reflectivity and overlapping flow fronts and edges, we estimate that much of the EPR crest, between 0–~2 km from the axis, in the 9° 25'–55'N area is surfaced by flows that are <1 kyr old. This compares to a mean spreading-based age of ~40 kyr for ocean crust at a distance of 2 km from the AST.

6. THE AXIAL SUMMIT TROUGH AND HYDROTHERMAL VENTS AT THE EPR 9° 46'–51'N

The primary fissure system of the 1991 eruptive event is characterized by a relatively continuous, 1–3 m-wide fissure usually located along the center of the AST (Plates 3, 5, and 7a–f) [Haymon *et al.*, 1993; Gregg *et al.*, 1996; Fornari *et al.*, 1998a]. The fissure has an en echelon form and occasionally steps laterally a few meters, such as the right lateral offset of ~2–3 m near the Bio9/9' vents [Shank *et al.*, 1998]. The depth of the fissure has been observed to be from ~1 m to >3 m, beyond the visual field of view from Alvin's viewports. However, scanning altimeter data show the fissure can extend to a depth of >~7 m, the limit of the sonar's beam. The morphology of the primary eruptive fissure system exhibits many features that reflect its formation and evolution. Often, there is extensive platy talus along the fissure; the talus plates generally are draped along the margin of the fissure, suggesting formation during drainback (Plate 6).

In places, the fissure is filled with sheet flow talus forming a chaotic assemblage of tabular lava fragments that is the substrate for animal communities often found along the axis and sides of the fissure system (e.g., BioMarkers 82, 119 and 141 biological communities [Shank *et al.*, 1998]) (Plate 3). Because of the chaotic nature of the lava flows, primary fissure, and extensive lava pillars along the AST wall throughout the study area, it has been difficult to get a broad, overview of the morphology of the terrain and to relate the vent sites and their edifice morphology to the surrounding volcanic features. The sidescan sonar and micro-bathymetry permit us to correlate the hydrothermal and volcanic features unequivocally for the first time.

The fundamental physical relationship between the eruptive volcanic fissure, the underlying zone of diking and seafloor exposures of hydrothermal fluid egress from the crust is well defined for the 9° 46'–51' N area. Plates 2, 3 and 5 show the spatial relationships between the high- and low-temperature vents within the AST in this area. Plate 5 shows the locations of three of the most vigorous high-temperature hydrothermal vents near 9° 50' N (Bio9, Bio9' and P vents), and their close association with two of the most prominent channels in the AST wall adjacent to these vents. These channels interrupt the continuity of the AST wall and are presumed to represent 'breakouts'; where erupting lava has breached the wall and flowed down slope.

Nearly all the hydrothermal vents shown on Plates 2, 3 and 5 are located along the floor of the AST and most occur within or proximal to primary eruptive fissures that fed the 1991 eruption [Haymon *et al.*, 1993; Rubin *et al.*, 1994; Gregg *et al.*, 1996; Shank *et al.*, 1998; Fornari *et al.*, 1998a] (Plates 8–9). This area has been intensively studied since the 1991 volcanic eruption. We have a good understanding of the general location of high- and low-temperature vents and their associated biological communities and of their relationships to ridge segmentation, morphology, and basalt geochemistry [e.g., Haymon *et al.*, 1991, 1993; Perfit *et al.*, 1994; Lutz *et al.*, 1994; Fornari *et al.*, 1998a; Shank *et al.*, 1998; Mullineaux *et al.*, 1998; Perfit and Chadwick, 1998; White *et al.*, 2002; Haymon and White, in press]. In addition, fluids from these vents have been regularly sampled over the past ~10 years [e.g., Von Damm, 2004 (this volume and references therein)]. Continuous time-series temperature measurements have also been acquired providing a historical baseline for the fluid characteristics of individual vents and their variability with time. [e.g., Fornari *et al.*, 1998b; Fornari and Shank, 1999; Scheirer *et al.*, submitted, Shank *et al.*, submitted],

There are two distinct clusters of high-temperature vent fields in our study area, one at ~9° 50' N and one at ~9° 47' N (Plates 2–3). The distance between these two areas is ~7 km and simple geometric considerations as well as vent fluid chemistry suggest that vents in these two areas are primarily fed by fluid convection cells, each with its own water-rock reaction zone. Exit fluid compositions are also highly variable between individual vents within each field [e.g., Von Damm *et al.*, 1995, 1996 1997; Oosting and Von Damm, 1996; Von Damm, 2000, 2004 (this volume); Ravizza *et al.*, 2001; German and Von Damm, 2004], as well as between the two adjacent fields, demonstrating that subsurface flow conditions can vary despite close proximity between exit orifices. The high temperature hydrothermal vents located between 9° 49'–51' N fall into two categories based on their spatial relationship with the AST (Plates 3 and 5). Biovent, M and Q

vents are situated along or just outside the AST walls and we presume that fluid pathways are largely controlled by fractures associated with the margins of dikes intruded along the trace of the AST. Tica, Bio9, Bio9', P, Ty, Io and Tubeworm Pillar (TWP) vents are all located within the floor of the AST, along the primary fissure system. A brief summary of the salient characteristics of each, based on observations made from Alvin between ~1991–2002 follows.

Biovent, the northernmost high-T vent in our study area, is located near 9° 51' N on the western rim of the axial trough (Plates 2, 3 and 8a). Based on towed camera and Alvin dive observations, it is the only high-T vent on the EPR crest between ~9° 51' N and 9° 55' N. In 1995, self-recording temperature probe data [Fornari *et al.*, 1998b] (N.B. probes have resolution of $\pm 1^\circ\text{C}$) indicate Biovent fluids were 352°C. In 1997, fluid temperatures at this vent were 343°–345°C and at the end of the recording period, in September 1998, Biovent fluid temperatures had decreased to 341°C [Fornari *et al.*, 1998b; Von Damm, 2000]. In January 2002, Biovent fluids measured 345°C.

M vent, the next vent south of Biovent, is located on the eastern wall of the axial trough at 9° 50.8' N (Plates 3, and 9b–c). In 1995, M vent fluid temperature based on self-recording probe data was 358°–360°C (Alvin high-T probe measured 365°C). The time-series fluid temperature record for this vent is extraordinary in that we see no variations greater than a few degrees, or within the 1°C resolution of the HOBO, self-recording probe [Fornari *et al.*, 1998b]. Alvin high-T probe temperature for M vent in May 1999 was 365°C. For 4 years, M vent fluid temperature recorded at 30 min intervals by the probes was constant at ~358°–360°C. The stability during this period is in marked contrast to the fluid temperature records for high-temperature vents south of M in the Bio-Transect. In January 2002, M vent fluids ranged from 369°–374°C. Q vent, just south of M vent on the eastern AST wall, has not been instrumented successfully although it has been repeatedly sampled for fluids [Von Damm, 2000, 2004].

Tica vent lies within the center of the AST floor along the primary eruptive fissure, between the M/Q vent area to the north and the Bio9/9'/P vent complex to the south (Plates 3, 5, and 8d). This hydrothermal site consists of vigorous, low temperature diffuse flow which has supported ~13 discrete patches of tubeworms since 1997. The vent field measures ~30 x 60 m and occurs on pressure ridges formed in lobate and ponded flows in the center of the AST floor. High temperature venting at this site appears to have begun only recently, within the last 2 years. In December 2003, the recorded temperature of fluids from the ~2 m tall black smoker chimney at Tica was 342°C. The ~2 m-wide flat-topped sulfide structure is located towards the southern end of the field with extensive colonies of *Alvinella pompejana* and *Alvinella caudata* poly-

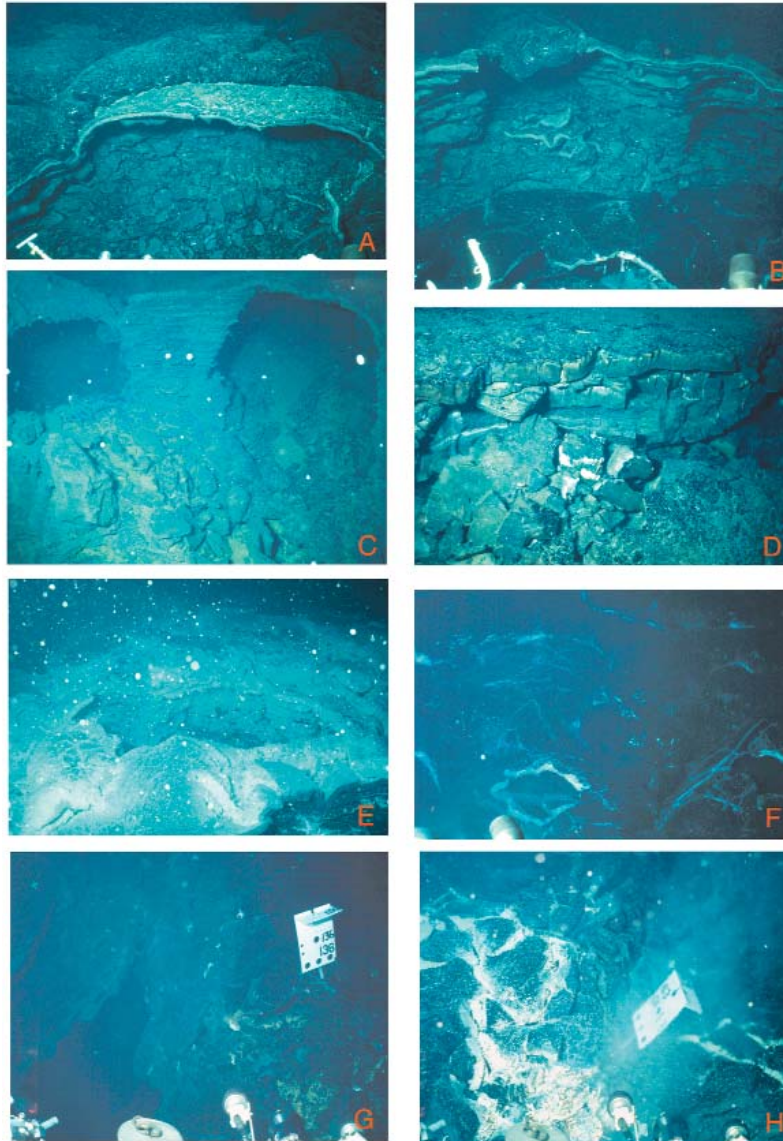


Plate 7. Volcanic morphology on the floor and walls of the AST in the $9^{\circ} 50' \text{N}$ area as imaged by *Alvin*. Scale in meters across the foreground of each photograph is given in brackets at the end of each description. (A) Collapse blister in lobate flow with 1991 lava mantling the top of the blister [2]. This example underscores the potential for intra-flow permeability in the fast-spreading MOR environment where lava flows can effectively seal off large water-filled cavities in the underlying flows. (B) West rim of the AST showing top surface of fresh, glassy 1991 lava (lower edge of photo) just below the rim [3]. Note that the 1991 flow is also collapsed (bottom center of photo). (C) Lava tube/archways in the wall of the AST [3]. (D) Rim of AST showing thin flow units and small gaps between flows. This is an example of intra-flow permeability. Bottom right corner of photo shows a collapsed portion of the wall, tilted into the AST [2]. (E) Collapse pit just outside the rim of the AST (lower right corner) with extensive coating of bacterial matter. This is an example of inter-flow permeability and underscores the high potential for fluid flow through large drainback and collapse-generated void space within lobate and sheet flows at the EPR in this area [3]. (F) Glassy 1991 lobate lava showing small windows in lobes indicating the flow is partially water-filled; another example of intra-flow permeability [1.5]. (G) Well-defined actively venting primary eruptive fissure adjacent to Biomarker 136 continues to vent since deployment of the marker in 1992 [3]. Note platy talus beneath marker that dips in towards the axis of the fissure. (H) North of Biomarker 63 the fissure system was less well defined adjacent to Biomarker 63, but was also actively venting in 1992 as seen here, and supported a small tube worm community [2]. Twenty-one months later, this fissure was inactive.

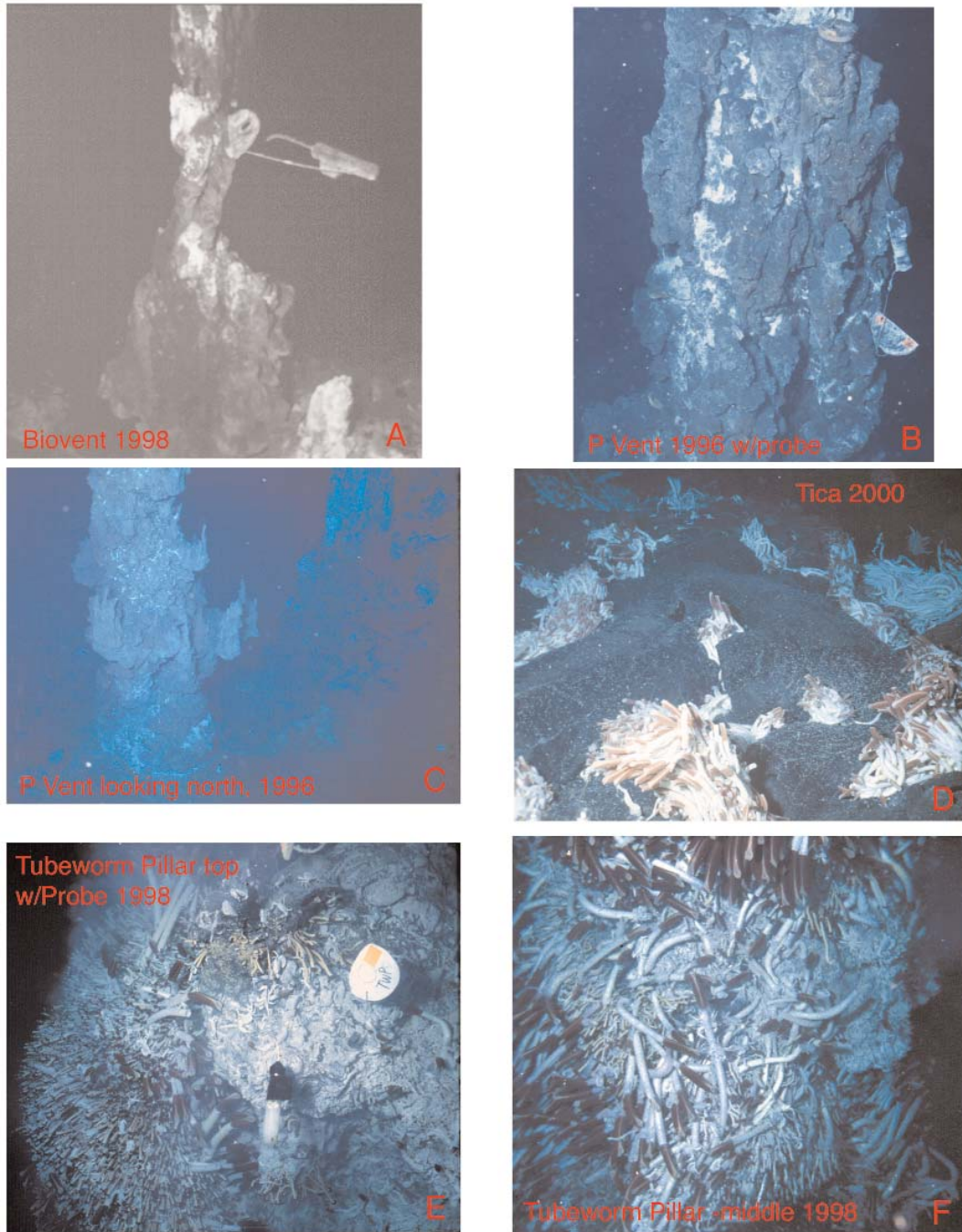


Plate 8. Chimney structures of various high-temperature hydrothermal vents in the $9^{\circ} 49' - 51' N$ region of the EPR as imaged from *Alvin* (see Plates 2, 3 and 5 for locations). Scale in meters across the foreground of each photograph is given in brackets at the end of each description. (A) Biovent in 1998 [1.5]. (B) P vent with HOBOTemperature probe (lower right) in 1996 [2]. (C) P vent mound comprising 3 primary chimneys on top of the sulfide rubble mound constructed along the primary eruptive fissure as viewed from the northwest in 1996. P vent is normally sampled at the southernmost chimney [4]. (D) TICA diffuse flow biological community located at $9^{\circ} 50.4' N$ in lobate lavas on the floor of the AST [2]. (E) Top of Tube Worm Pillar in 1998 showing HOBOTemperature probe in the black smoker vent at the summit of the ~ 10 m-tall edifice [2]. (F) Middle portion of Tube Worm Pillar in 1998 showing assemblage of *Riftia*, *Tevnia* and other biological constituents that are bathed by warm hydrothermal fluids that seep out of the sides of the pillar [2].

chates thriving from almost the base to the top. *Cyanograea* crabs and *Hesiolyra* polychaetes were also present. In December 2003, the *Riftia pachyptila* populations surrounded Tica vent, extending from the basalt around the base to over the height of the vent. No long-term temperature studies have been carried out at Tica.

Three high-T vents within the AST are located near the northern limit of the BioTransect area ('Hole-to-Hell' locale of *Haymon et al.*, [1993]): Bio9, Bio9', and P vents [*Shank et al.*, 1998; *Fornari et al.* 1998b; *Von Damm and Lilley*, 2003, *Von Damm*, 2000, 2004 (this volume)] (Plates 2–3, 5, 8b, and 9d–f). Bio9' and Bio9 vents are located within a ~5 m of each other along the primary eruptive fissure of the 1991 eruption [*Haymon et al.*, 1993; *Fornari et al.*, 1998a,b]. P vent is located ~40 m south of Bio9 vent and consists of a sulfide mound ~1–3 m tall that has grown along the primary eruptive fissure and upon which there are typically three principal chimney structures. Traditionally, fluids and temperature measurements from this small complex are sampled at the southernmost chimney. While Bio9/9' have had extensive tubeworm communities developed in the areas immediately surrounding the vents and on the adjacent eastern wall of the AST, P vent is largely devoid of *Riftia* tubeworm communities [*Shank et al.*, 1998]. Both vent areas have had extensive areas of bacterial mats and Alvinellid communities on the surfaces of the high temperature chimneys [*Shank et al.*, 1998; *Von Damm and Lilley*, 2003]. The most extensive time-series exit fluid temperature data exist for the Bio9 vent; and to a lesser extent, Bio9' and P vents. Selected exit fluid temperature data for the Bio9 vent and other vents within the BioTransect are shown in Plates 10 and 11.

There are three other high-T vents in the BioTransect [*Shank et al.*, 1998]. Ty and Io vents became active in 1997 and are located ~250 m south of P vent, near the Marker 82 diffuse flow biological community [*Shank et al.*, 1998], in an area of jumbled sheet lava and drainback features along the primary eruptive fissure (Plate 5). Ty vent (Plate 9a) is located ~5 m north of Io vent, and in November 1997 it was a ~2 m tall chimney venting fluid at 352°C. The HOBO probe at Ty vent recorded data from November 1997 to September 1998 after which recording stopped due to low battery power [*Scheirer et al.*, submitted]. During the recording period, Ty showed a significant decrease in temperature (~10°C) that also coincided with the onset of the Bio9' and Bio9 temperature event in late November 1997 (Plate 11). Fluid temperatures at Ty vent continued to decrease until January 1, 1998 and then began a slow, steady rise back to pre-event levels. Alvin high-temperature probe measurements in May 1999 at Ty show the fluid temperature was 352°C; in January 2002, it measured 350°C [*Scheirer et al.*, submitted]. In 1997, when Io first became active, it was a 1–2 m tall, ~1 m diameter

stump of diffuse flow and hotter (~100°C) venting fluids. When visited in May 1999, Io was a ~9 m tall, ~2 m diameter edifice vigorously venting hot, diffuse fluid over its entire surface area. At that time, 348°C fluids were venting from orifices at the top of the structure, including some orifices that had classic "beehive" sulfide caps. Io fluid temperatures had reached 356°C by Jan. 2002 [*Scheirer et al.*, submitted].

Ty, Io and Damoclese Sword vents, located ~300 m south of Bio9/9' and P vents, are also flanked to the east by a small breakout channel along the east rim of the AST (Plates 3 and 5). There are hints in the sonar data that a similar channel exists to the west of the Ty/Io area but the vehicle nadir obscures the character of the west margin of the AST at this site. The Ty/Io vents are near the middle-eastern side of the AST which is only ~60 wide in this location; Damoclese Sword vent is just inside the east wall of the AST. The primary eruptive fissure widens in this area and low-temperature diffuse flow, and vent animal colonization has occurred along the fissure several tens of meters north and south of the black smoker vents since the 1991 eruption; one of the primary biological sites is BioMarker 82 (Plate 5) [*Shank et al.*, 1998].

The southernmost vent in the study area is located at the top of Tube Worm Pillar (TWP) (Plates 5 and 8e–f). TWP is a large lava draped edifice (~10 m tall, ~2–3 m diameter) at the southern end of the BioTransect [*Shank et al.*, 1998] and hosts a large vestimentiferan tubeworm community on its sides and top. TWP was active in 1989 and 1991 (before the 1991 eruption). In 1992, TWP was venting 160°C fluids, and it rapidly became a black smoker by 1993 when it was sampled and fluid temperatures were measured at 351°C. Since then, fluid temperatures at this vent have dropped steadily and the number of tubeworms on its sides has decreased dramatically. When visited in January 2002 the exit fluids were only 186°C [*Scheirer et al.*, submitted] and in April 2004 there was no active black-smoker on TWP.

7. DISCUSSION

We hypothesize that breakout channels (Plates 3 and 5) along the AST walls can serve as long-term (10s to 1000s of years) controls on lava distribution at the EPR [*Schouten et al.*, 2001, 2002]. Studies of channelized submarine sheet flows and of the quantitative distribution patterns of various lava morphologies within the AST and around hydrothermal vents provide important first-order constraints on: 1) MOR volcanic effusion rates [e.g., *Gregg et al.*, 1996; *Gregg and Sakimoto*, 2001; *Parfitt et al.*, 2002], 2) the style of volcanic emplacement [e.g., *Embley and Chadwick*, 1994; *Fornari et al.*, 1998a; *Chadwick et al.*, 2001; *Chadwick*, 2003; *Engels et al.*, 2003], and 3) their role in creating shallow crustal fluid flow pathways that utilize volcanically induced permeability

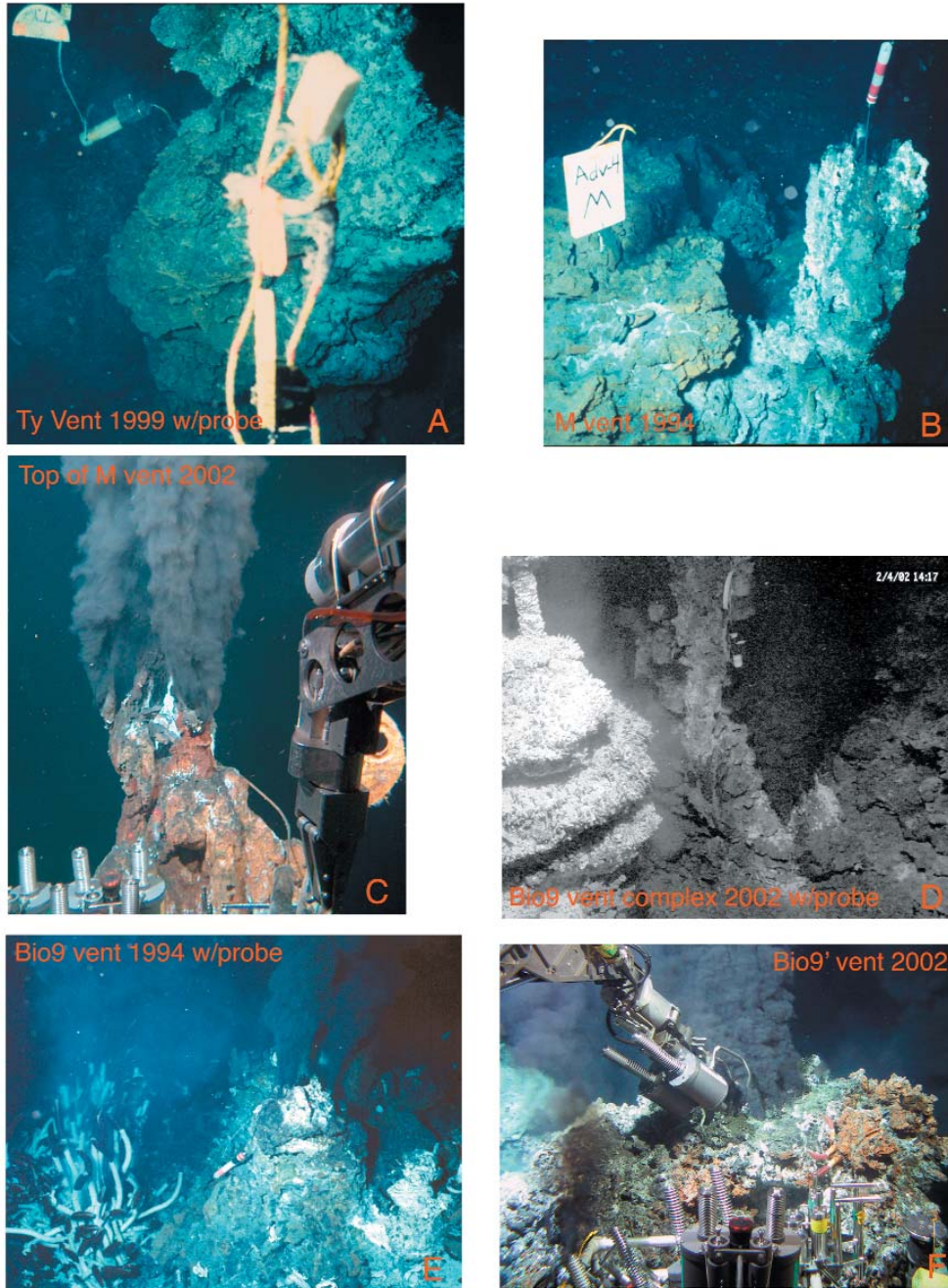


Plate 9. Chimney structures of various high-temperature hydrothermal vents in the $9^{\circ} 49' - 51' N$ region of the EPR as imaged from *Alvin* (see Plates 2-3 and 5 for locations). Scale in meters across the foreground of each photograph is given in brackets at the end of each description. (A) The middle portion of Ty Vent in May 1999 with HOBOT temperature probe installed. This photo was taken before the probe was extracted from the chimney wall [3]. (B) M vent in 1994 with HOBOT temperature probe installed. The marker at left center is sitting on lobate lava at the rim of the AST, vent edifice is growing from a fracture in the upper portion of the AST eastern wall [2]. (C) Top of M vent in 2002. The tubing from a HOBOT probe can be seen just below the right set of black smokers [1]. (D) Bio9 vent complex in 2002. HOBOT probe can be seen inserted in chimney orifice in top center of photo [3]. (E) Bio9 vent in 1994 showing HOBOT probe installed and developing Riftia tube worm community at left, along the margin of the primary eruptive fissure of the 1991-1992 eruption. (F) Bio9' vent in 2002 during sampling using a titanium 'majors' bottle [1].

structure within and between lava flows. The volcanic stratigraphy within the AST and within the shallow crust plays an important role in determining the fluid pathways that serve to mix high-temperature hydrothermal effluent with ambient seawater—resulting in the diffuse flow fluids that bathe animal communities at sites surrounding the high-T vents. We suggest that areas where channelized volcanic flows have breached the rim of the AST are also the primary eruption centers for the 1991 lava and the sites of extensive post-eruption drain back of lava into the primary fissure. These localized sites where the eruptions focused and drainback occurred along the fissure in the floor of the AST provide important controls on shallow crustal permeability and vent fluid pathways. These environments are likely to localize low- and high-temperature hydrothermal venting and may influence reaction zones for low-temperature fluids, thereby impacting the colonization and development of biological communities.

Many authors have reported on the close association of fresh volcanic terrain, fissures and faults in an intermediate to fast-spreading MOR axial zone with hydrothermal venting [e.g., Ballard *et al.*, 1979; Francheteau and Ballard, 1983; Delaney *et al.*, 1992, 1997, 1998; Haymon *et al.*, 1991, 1993; Wright *et al.*, 1995a,b; Wright, 1998; Curewitz and Karson, 1998; Fornari *et al.*, 1998a; Embley *et al.*, 2000; Chadwick *et al.*, 2001; Chadwick, 2003]. What is pertinent to the present discussion is the extent to which locations of specific hydrothermal vent sites can be related to primary volcanic features (e.g., eruptive fissures and vents, collapse features, channels, lava tubes, etc.) (e.g., Plate 6) or tectonic features, and if these spatial associations are linked to spreading rate and ridge crest morphology/structure.

For example, Embley *et al.* [2000] and Chadwick *et al.* [2001] provided detailed submersible and remotely operated vehicle (ROV) observational data to link locations of hydrothermal vents formed during the 1993 CoAxial eruption (e.g., Source and Floc sites) to fissures and grabens developed above the intruded dike. In other examples along the Juan de Fuca, field relationships show that the locations of hydrothermal vents (e.g., Monolith vent) can be related primarily to narrow zones along fissures and small (~20 m wide) graben developed as a result of the stress field imparted by the intruded dikes [Chadwick *et al.*, 2001]. At intermediate spreading MORs, the deeper depth to the magma lens (~2–3 km) [e.g., Morton *et al.*, 1987; West *et al.*, 2001], compared to the shallower magma lens depth (~1.5 km) beneath the EPR [e.g., Detrick *et al.*, 1987; Sinton and Detrick, 1992; Kent *et al.*, 1993; Harding *et al.*, 1993], and the structural regime in the ~2–4 km wide rift valley—with its prevalence of tensional fractures and faults—provide a more distributed system of vertical pathways for hydrothermal fluids to exit the crust. The recent near-bottom magnetic surveys of the Main Endeav-

our Hydrothermal Field (MEF) [Tivey and Johnson, 2002] point to the presence of well-defined magnetic lows suggesting vertical ‘pipes’ spaced ~200 m apart where primary hydrothermal upflow is concentrated in the Endeavour rift valley. High-resolution near-bottom multibeam data for the MEF [Johnson *et al.*, 2002; Tivey *et al.*, 2003], when combined with the *in situ* and magnetic data, clearly show the primary fault influence on distribution of the vents in this intermediate-spreading MOR setting.

Based on our interpretation of the micro-bathymetry and sidescan sonar data, and visual and photographic observations of this terrain we concur with Haymon *et al.* [1993] and Wright *et al.* [1995a, b] that the first-order control on hydrothermal vent localization and vertical fluid flow pathways within the axial trough in the study area are provided by the 1991 eruptive volcanic fissures within the EPR AST between 9° 46′–51′N, and the underlying feeder dikes. Our working hypothesis is that the seafloor locations of active hydrothermal chimneys in this area are located where the eruption focused along the fissures and where drainback of magma occurred. The permeability structure of the uppermost crust at these sites is likely to be enhanced because of the repeated cycles of waxing and waning of eruptions within the magmatic conduits and interactions with seawater vapor during eruptions [Perfit *et al.*, 2003]. Only Biovent, M and Q vents are located along the bounding wall or at the rim of the AST. All the other high-temperature vents within the AST are located along the trace of 1991 eruptive volcanic fissures that lie near the center of the trough floor (Plates 3 and 5). For the vents near 9° 46′–47′N (Plates 2–3) about half are located within the AST and the rest are located along the west wall of the trough [Von Damm *et al.*, 1995].

We suggest that the locations of seafloor vents that comprise hydrothermal systems at 9° 50′N are being guided by two primary geologic features. The first are fractures associated with the vertical to near-vertical dikes that fed the 1991 eruption. The second involves permeable zones created during the focusing of the eruptions and subsequent drainback of magma along the widest portions of the eruptive fissure and the ensuing chaotic mix of wall rock and platey talus fragments of new lava from the eruption that are rafted down the fissure. The area surrounding Bio9 was described by Haymon *et al.* [1993] as the ‘Hole to Hell’ because of the intense and turbulent hydrothermal flow exiting bare fresh basalt and extensive evidence for surficial hot rock-water interaction (Plate 6f), such as would be expected in a zone of active drainback during the waning stages of a seafloor eruption. Dike models and observational data suggest that where eruptive fissures are widest the greatest volume of magma erupts, although many factors can play a role in localization of magmatic flow in an eruptive fissure [e.g., Delaney and Pollard,

1982; Bruce and Huppert, 1989; Parfitt and Wilson, 1994; Wylie *et al.*, 1999]. Although evidence for drainback is often cited in descriptions of submersible-based observations of seafloor volcanic terrain at the EPR and Juan de Fuca it has not been directly related to hydrothermal vent localization [e.g. Fornari *et al.*, 1998a; Chadwick, 2003]. McClain *et al.* [1993] and Rohr [1994] suggest that volcanic drainback can be important in producing high permeability and anomalously low seismic velocities in shallow crust on the Juan de Fuca. The high-resolution sonar data and visual observations of the EPR AST terrain in the 9° 50'N area, and relationships discussed above provide correlative spatial information that can be used to relate eruption and volcanic processes with hydrothermal vent locations.

We propose that a combination of near surface dike position and narrow zones of permeability created by chaotic post-eruption drain back are providing a primary control on vent location and vertical fluid circulation above the water/rock reaction zone. The depth to the water/rock reaction zone in the study area based on chlorinity and silica geobarometry data [Von Damm, 2000, 2004] has varied over time since 1991. The calculated depth of the water/rock reaction zone was as shallow as ~150 m in the 9° 50'N area during the 1991 eruption and can be deep as ~1 km. Von Damm [2004 (this volume)] provides further evidence for the temporally variable nature of the reaction zone beneath the 9° 50'N "Hole-to-Hell" vents and their shallow depth based on the high temperatures of the venting fluids (~>350°C) and the corroborating Cl and Si data; which point to a reaction zone that is within the upper few hundred meters. This depth includes the calculated transition zone between upper extrusive sequences and sheeted dikes determined from geophysical data to be at ~ <200 m depth [Kent *et al.*, 1993; Harding *et al.*, 1993]. As Von Damm [2000, 2004 (this volume)] points out, clearly the heat source has been varying over the decade since the 1991 eruption, and there is ample suggestion based on recent vent chemistry and observations at these vents that magma may have been injected below the AST to shallow crustal levels above the magma lens. Magma injection and fluid flow through primary upper crustal fractures, which are likely to be reactivated frequently by the many micro-earthquakes in this fast-spreading environment, provide the primary control for transferring heat and chemical signatures to venting fluids.

We suggest that secondary control on the shallow fluid flow paths in the upper crust—which can be influential in modulating fluid temperatures and chemistry depending on geometry of flow paths results from the AST morphology, variable nature of seafloor volcanic morphology within the trough and the complex shallow stratigraphy of lava sequences that result in inter-flow and intra-flow porosity/permeabil-

ity. Studies that seek to develop hydrologic and thermal models of the shallow crustal permeability and tectonic/magmatic processes at the MOR [e.g., Wilcock, 1998, in preparation; Yang *et al.*, 1998; Lowell and Germanovich, 1994; Germanovich *et al.*, 2001] need to factor in the complex geometry imparted by the combination of volcanic eruption and lava distribution processes and the morphology of the axial zone as these have strong influences on the development of the geometry of fluid flow paths in the shallow crust at fast spreading MORs.

Near-bottom magnetic data may be one way to further constrain the nature of the permeability structure in the shallow crust at MORs. The magnetic maps in Plate 5 show a prominent low that is coincident with the axis of the axial trough suggesting very thin crust (lava) and the presence of shallow dikes. Elongate closed-contour lows around the northern vents (Bio9/9' and P) at 9° 50.3'N, and the Ty and Io vents near 9° 50.1'N suggest possible 'burn holes', that are smaller in diameter, but similar to, the near-bottom magnetic expression of vents imaged at JDF Main Endeavour Field [Tivey and Johnson, 2002]. Data shown in Plate 5c were collected along lines spaced 60 m apart; it is evident that more closely spaced lines are required to properly image the smaller EPR vent systems. The prominent magnetic high just west of the AST near 9° 50.4'N is likely to be a primary depo-center for the 1991 eruption and is coincident with the large breakout from the AST believed to be related to extensive drain back at this location, proximal to the locus of high-temperature venting at Bio9/9' and P vents.

The time-series temperature data available for the EPR 9° 50'N vents provide further insight into the issue of shallow fluid circulation and how closely spaced vents could have fluids with varying chemistry over time. For instance, in March 1995, the HOBO record for Bio9 vent (Plate 10) showed an abrupt temperature increase that has been correlated to a micro-seismic swarm [Sohn *et al.*, 1998, 1999; Fornari *et al.*, 1998b] that presumably resulted from fracturing in the lower crust induced by the evolving hydrothermal fluid circulation pattern and the resulting thermal stresses in lower crustal rocks. Time-series exit fluid temperature data indicate it took ~4 days for the effects of the cracking event to manifest themselves at the surface as an abrupt temperature increase [Fornari *et al.*, 1998]. Wilcock [2004] has modeled these data and shown that the magnitude of the increase and the time delay between the start of the seismic event and the observed increase in fluid temperature at the seafloor can be modeled using a pressure perturbation model. Wilcock's modeling predicts a temperature increase of 50°C in the reaction zone (~1 km depth [Sohn *et al.*, 1998, 1999]) and suggests that the physical dimensions of the crack transporting the fluids from depth is 0.6 mm wide (using laminar flow

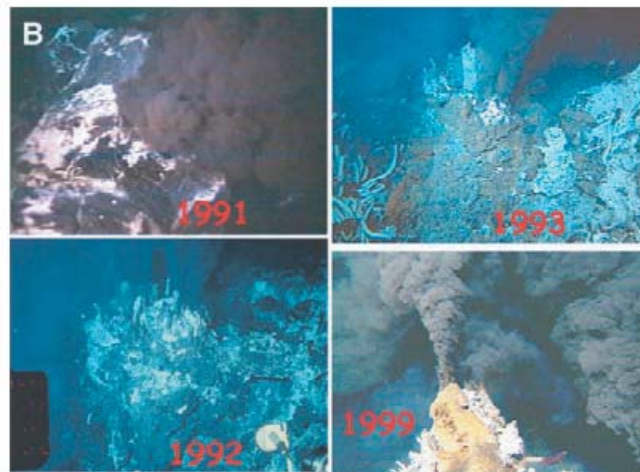
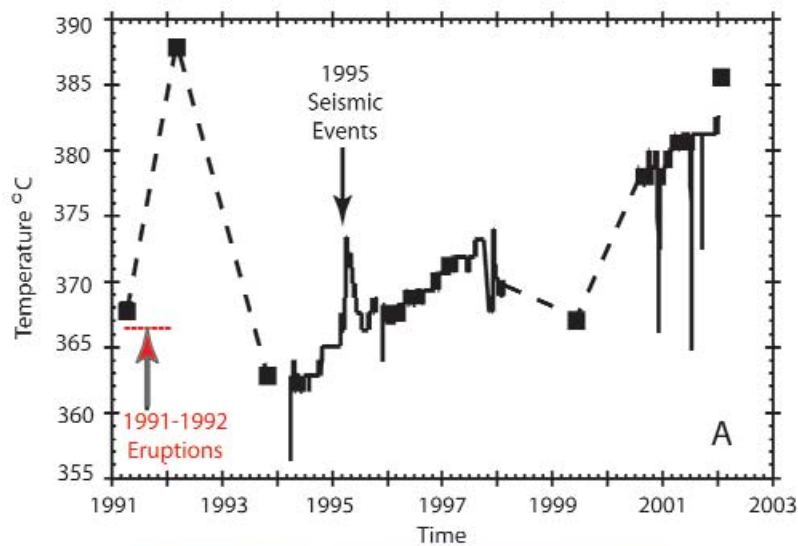


Plate 10. A) Time-series temperature data for the Bio9 high-temperature vent at the EPR near $9^{\circ} 50.1' N$ (see Plates 3-5 for location). Data were collected using the DSPL SeaLogger probes (continuous line) and Alvin high-T probe data (black squares), for intervals when the vent was being sampled for fluids and sulfides [Fornari *et al.*, 1998; Von Damm, 2004 (this volume)]. Intervals with no data are shown by dashed lines. DSPL HOBO SeaLogger probes have recorded the exit fluid temperature of this and other vents in the area every 30 min over the decade since the 1991–92 eruptions [Haymon *et al.*, 1993; Rubin *et al.*, 1994]. Note that there has been an overall rise in temperature at this vent since the 1991–92 eruptions, with present day temperatures being roughly equal to those measured in April, 1992 immediately after the 1991–92 eruptions. Based on these data and fluid and gas chemistry Von Damm [2000], Lilley *et al.*, [2003] and Von Damm and Lilley, [2003] suggest magmatic activity at this site is resurgent (K. Von Damm, pers. commun., 2003). B) Alvin bottom photographs showing the physical evolution of the Bio9 vent since 1991. Upper-left photo shows black hydrothermal fluid exiting bare basalt and bacteria covered seafloor during or just following the 1991 eruption [Haymon *et al.*, 199]. Upper-right, and lower-left photos show the small sulfide mound with multiple orifices that typified Bio9 vent during the 1992 to 1993 time interval. Tube worm community that developed around the base of Bio9 is visible in the left corner of upper-right photo. Bottom-right photo shows the smoke from Bio9 vent (right side of photo) and immediately adjacent Bio9' vent in 1999. By this time both vents had grown to be ~5–7m tall, ~1 m diameter chimneys vigorously venting black smoke. Scales across bottom of upper left and lower right photos are ~1.5 m. Scales across bottom of two two photos is ~2.5 m.

with a velocity of 1.2 m/s). *Von Damm* [2004] points out that the chemical data do not unequivocally constrain whether the cracking resulted from additional emplacement of magma or from hydrothermally induced cooling cracking into deeper, hotter rocks. Long term variations in exit fluid temperatures for the ‘Hole-to-Hell’ vents show the following trends. Since early 1995, fluid temperatures at the Bio9’ and Bio9 vents have increased from ~365°C to 372°C in November 1997. P vent fluid temperatures increased ~12°C, between November 1997 and May 1999. A general increase in Bio9’ and Bio9 (Plate 8) fluid temperatures of ~7°C was recorded between November 1997 and May 1999 [*Fornari and Shank*, 1999; *Scheirer et al.*, submitted].

Data presented in *Scheirer et al.* (submitted) provide longer time series information than the data shown in Plate 11, however, the temperature event recorded at Bio9 and Bio9’ vents and the adjacent Bio9 Riftia diffuse flow community in the time period November 28 to December 17, 1997 area useful in illustrating how the shallow fluid circulation system feeding adjacent vents is complex and how the setting of the vent (i.e., within the floor of the AST or on the AST wall) impacts primary hydrologic feeders (Plate 11). The November 28 event caused a sharp rise in the exit fluid temperature at Bio9, Bio9’ and in the low temperature biological community adjacent to the Bio9 chimney (Bio9 Riftia). M vent, which is located ~1 km north of Bio9 (Plate 3) on the east wall of the AST saw no change to its fluid temperature which was steady at 357°C. Biovent, also ~1.2 km north of Bio9 saw no change in its fluid temperature which was steady at 343°C. P vent, only ~40 m south of Bio9 also shows no change in its temperature of 372°C despite the close proximity to the Bio9 plumbing system. The probe in Ty vent, ~300 m south of Bio9, does show an effect from the event but it is recorded as a steady drop in the fluid temperatures which had been at 331°C prior to the event and eventually dropped to ~321°C after about a month, whereupon the temperature recovered to pre-event levels (Plate 11). All told, the data suggest a complexity in fluid circulation that is difficult to reconcile with a simplistic fluid circulation model that has strong spatial links between limbs of the plumbing system. While the lack of a thermal effect on the M and Biovent fluids from the November 28 event is easy to understand in light of both the spatial separation between them and Bio9 and their different setting along the AST, the lack of effect on P vent fluids is confounding. The artist’s drawing presented in Plate 12 attempts to conceptually show the differences in fluid circulation in the shallow crust beneath the 9° 50’–51’ N vents that could cause the types of spatial/temporal variations observed in the time-series temperature data.

The full data set presented in [*Scheirer et al.*, submitted] show that four probes recorded several discrete periods (last-

ing a few days at most) where the Bio9’ vent fluid temperature dropped 3°–7°C, and took several weeks to a few months to recover to the value prior to the temperature drop. These types of variations were not observed in the fluid temperature record for the adjacent Bio9 vent during the same periods. Collapse of the Bio9 chimney, was recorded by a probe on February 6, 1998. This resulted in the expulsion of the probe from the vent orifice and its burial in the sulfide rubble that also impacted the Bio9 Riftia community just west of the vent (also instrumented with a Vemco, low-temperature recording array; part of that record is shown in Plate 11). In January 2002 Bio9, Bio9’ and P vent fluids measured 386°C [*Scheirer et al.*, submitted]. Taken together the diverse fluid temperature responses of these closely spaced vents suggest that they are not well connected hydraulically in the shallow crust.

As mentioned earlier, the very narrow width of the AST and the presence of all but one (Biovent) of the high-temperature hydrothermal vents in the floor or on the wall of the AST in the study area suggests that the up flow limb of hot fluid circulation is tightly constrained to the narrow zone of intrusion beneath the AST (Plate 12). At 21°S EPR, the Rapa Nui vent field consists of a complex of black smoker vents that dominates the western wall of the ~600 m wide axial graben. At Brandon vent, the well-established vertical pathways afforded by the tensional fractures within the upper crust, as a by-product of dike intrusion, are localizing the primary hydrothermal fluid exit from the seafloor. The intensity of venting, the high exit fluid temperatures (>400°C), and the observation of phase-separation at these vents [*Von Damm et al.*, 1998] suggest that the pathways from the rock-water reaction zone are near-vertical; none of the energy is being lost by lateral transport in the hydrothermal plumbing system in the lower or upper crust. Although on a much smaller scale, the ‘Brandon’ scenario is what we envision for Biovent, M, and Q vents. That is, focused hydrothermal flow along vertical pathways constrained by the tensional fractures above the narrow dike zone, with little complication of the flow geometry imparted by intra-flow and inter-flow permeability, such as is prevalent beneath the AST floor. The high concentrations of magmatic volatiles (e.g., CO₂, He, H) sampled in hydrothermal fluids at Biovent, M and Q vents within ~2 years of the eruptions supports the notion that they were greatly affected by the 1991 volcanic event and suggests direct hydrologic connections between the upper mantle, magma lens and water/rock reaction zone beneath this portion of the axis [*Lilley et al.*, 2003; *Lupton et al.*, 1993; *Von Damm*, 2000].

We do not have micro-bathymetry data from the area around Q, M and Biovent so we cannot speculate on the small-scale morphological associations between their locations and the

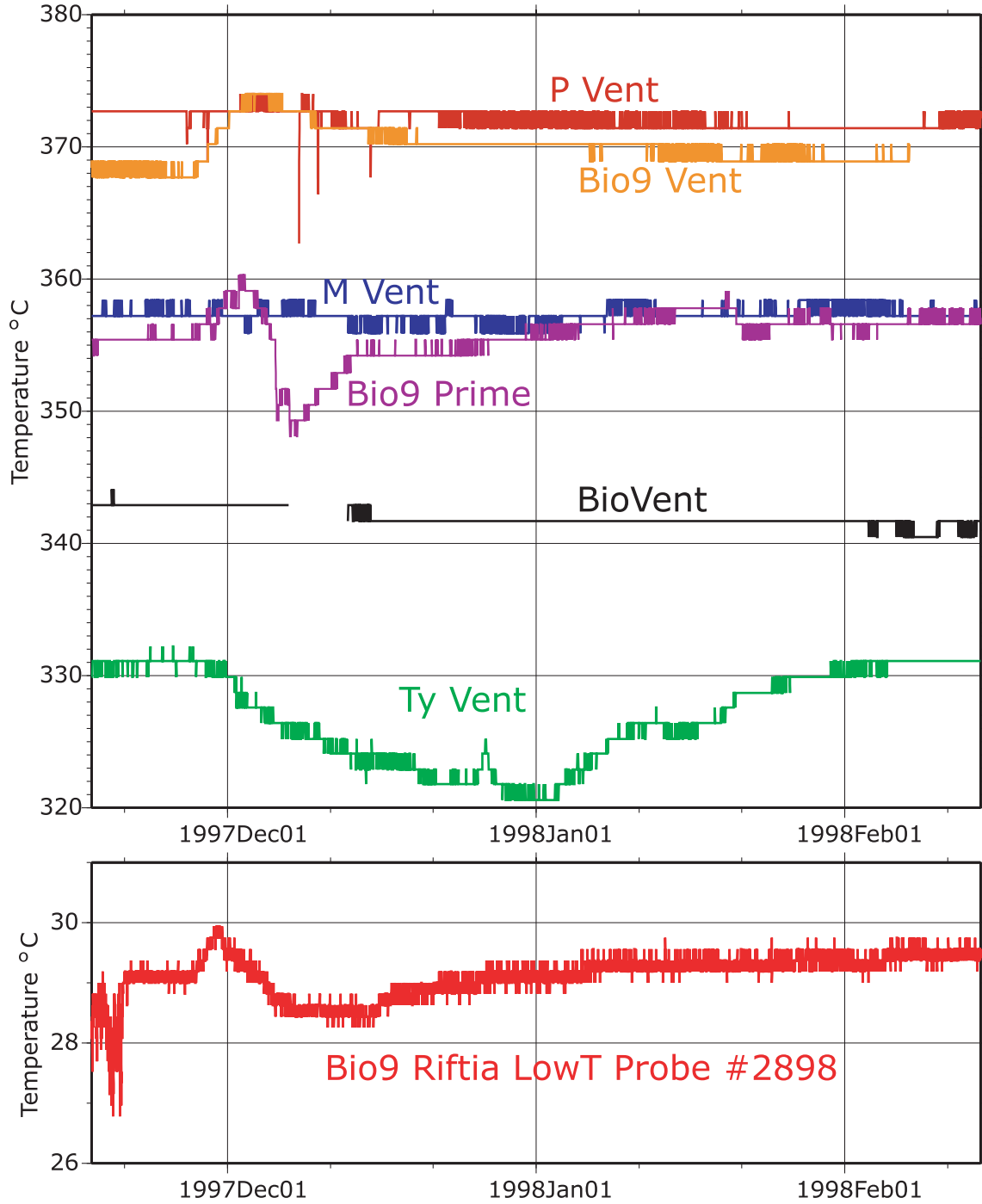


Plate 11. (Top) Detail of high-temperature HOB0 probe data [Fornari, *et al.*, 1994, 1996] for the interval between November 1997 and February 1998 showing temperature fluctuations at Bio9, Bio9'. Resolution of HOB0 probes is 1°C, data were recorded every 30 minutes [Fornari *et al.*, 1998b]. (Bottom) Vemco low-temperature logger data [Fornari, *et al.*, 1996] for the Bio9 *Riftia* community for the same time period showing temperature increase in late November 1997 that is coincident with the fluctuations in high-temperature fluids from the adjacent vents (see Plate 5 for vent locations). Red bar shows time period corresponding to the high-temperature records shown above. Resolution of Vemco probes is 0.1°C and data were recorded every 15 minutes.

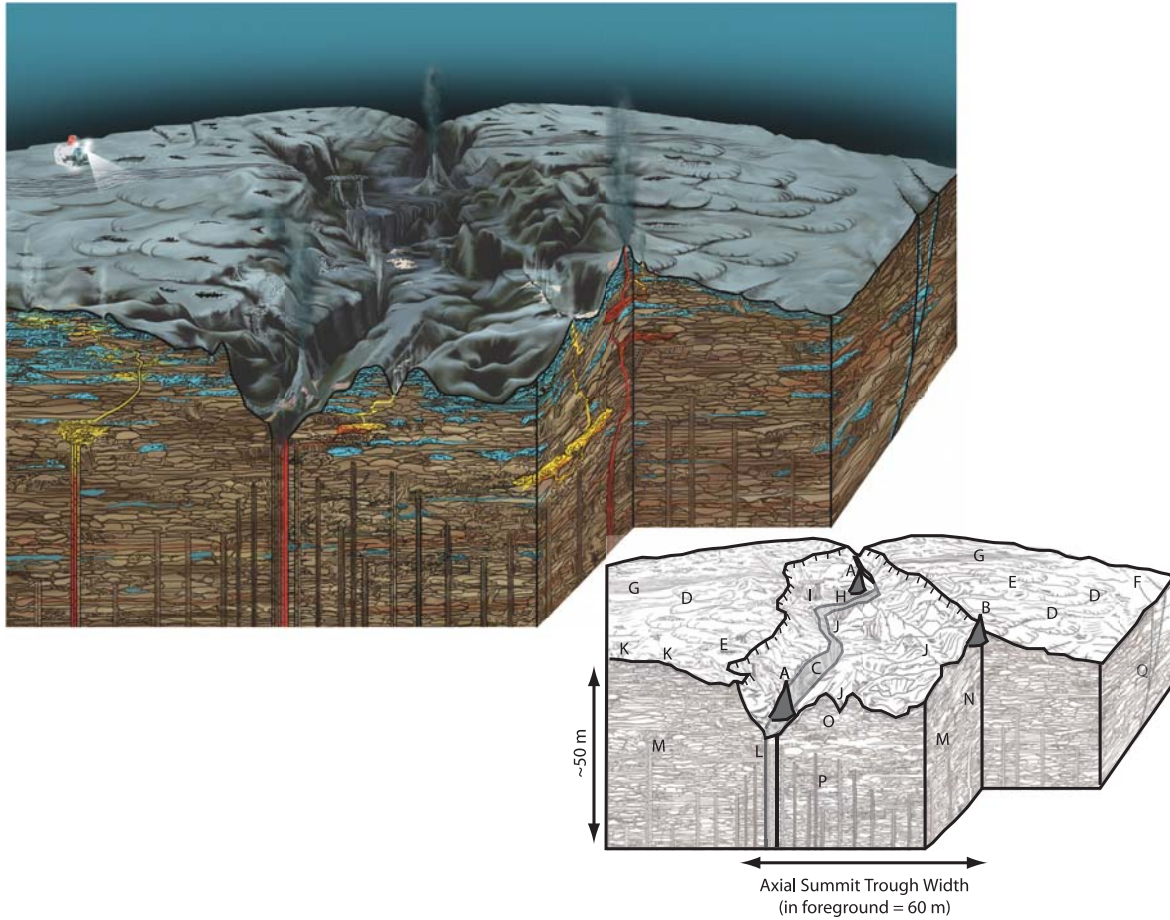


Plate 12. Artist's perspective of the East Pacific Rise crest in the $9^{\circ} 50' N$ area based on Alvin observations, ABE and Alvin near-bottom sonar mapping, and DSL-120A sidescan sonar imagery. All red, yellow and blue colors shown in the colored cross-section represent fluid temperatures with red being high-temperature ($>350^{\circ} C$) and blue low temperature ($<20^{\circ} C$). The interior structure is inferred based on observations in juvenile subaerial volcanic terrain in Hawaii and Iceland and from seafloor observations made using Alvin and a towed deep-sea camera system. Lettered inset at lower right provides key to various features drawn. A) High temperature vents along primary fissure in the axial summit trough (AST) fed by hot fluids that follow most recent eruptive dikes. B) High temperature vent along the bounding wall of the AST (e.g., M vent, Q vent) that taps fluids flowing through vertical fractures. C) Primary eruptive fissure within the floor of the AST. D) Scalloped flow fronts representing recent eruptions from the AST that flowed down the upper slopes of the EPR crest. E) Collapse pits of various sizes [see *Engels et al.*, 2003], with a focused zone of collapse within ~ 300 m to either side of the AST. F) Small throw (<5 m high) faults located usually ~ 1 km from the AST. G) Lava channels on either side of the AST that transported lava from an eruption source within the AST out to 1-2 km from the axis (Alvin, not to scale, shown at left). H) Drainback feature within the floor of the AST located along the primary fissure. This is believed to also be a site where the eruption focused. I) Lava pillar. J) Sites of diffuse hydrothermal flow at low temperature ($\sim <20^{\circ} C$) along the primary eruptive fissure. K) Sites of diffuse hydrothermal flow at low temperature ($\sim <20^{\circ} C$) outside the AST. L) Sub-surface trace of most recent eruptive dike. Hot (red) hydrothermal fluids are mining the heat from the dike and the magma lens below. M) Older dike that is sustaining hydrothermal flow that eventually feeds sites of off axis diffuse venting. N) Recent dike below the margin of the AST that feeds high-temperature black smoker vent situated along the AST wall (e.g., M or Q vents). O) Area of mixing of seawater and high-temperature fluids within fragmental and porous shallow volcanic layer to create hybrid hydrothermal fluids. P) Intruded dikes below AST of various age. Q) Site of off axis recharge of seawater into the shallow crust. (Drawing by E. Paul Oberlander – WHOI).

AST volcanic structures. However, analysis of the sidescan data for the area between 9° 50'N and 9° 51'N along the AST (Plate 2) suggests that Q, M and Biovent are not directly associated with extensive breakout channels from the AST or drainback, such as has been noted for Bio9/9', P, Ty, Io and Tube Worm Pillar vents further south (Plate 5).

8. SUMMARY

Focusing of volcanic eruptions, waxing and waning during eruptive phases and subsequent drainback of lava in a deep-sea setting has the potential to create fragmental and jumbled lava with high permeability within a steep sided, laterally restricted conduit that could then be utilized by upwelling, hot hydrothermal fluids (Plate 12). The geometry of shallow crustal permeability within the EPR axial trough in the 9° 50'N region is thought to be mainly controlled by the primary eruptive fissure network within the axial trough and the intersection of it by pipe-like structures where the eruptions have been focused and where drainback of lava localized. Areas of focused drainback are also likely to be centers of magma injection into the shallow crust. Jumbled sheet flows, breakout channels, collapse pits, and lava tubes act to transport and mix hydrothermal fluids in axis-parallel and axis-orthogonal directions within interfingering zones of high permeability. This complex subsurface structure may facilitate the development of hydrologic gradients that are utilized by hydrothermal fluids having various densities and temperatures which lead to hybrid fluids that bathe low-temperature animal communities.

High-resolution bathymetric and sidescan sonar maps of the AST in the EPR 9° 50'N area show spatial correlations between sites where the 1991 eruption is likely to have focused, creating channelized flows that transported the lava away from the AST, and active hydrothermal vents. We suggest that vent locations within the EPR axial trough are linked to formation of discrete, high permeability zones created by focusing of eruptions, cyclicity during eruptions, and subsequent drainback of lava into the primary fissure within the axial trough during waning stages of eruptions. Our new data confirms previous interpretations that current sites of hydrothermal venting are principally related to the trace of the fissure that fed the 1991 eruption. Drainback of lava in a deep-sea setting and magma/seawater interactions [e.g., *Perfit et al.*, 2003] have the potential to create fragmented and jumbled lava with high permeability within a steep sided, laterally restricted conduit that can be utilized by upwelling, hot hydrothermal fluids. The lateral extent of high-permeability regions is complex and may be limited by subsequent infilling of void space by younger lava. Frequent micro-earthquakes at fast-spreading MOR sites act to disrupt hydrothermal mineralization in small

veins within the crustal section which helps maintain permeability. Black-smoker hydrothermal vent locations and differences in time-series temperature history and chemistry between closely spaced vents reflect primary volcanic control on the geometry of fluid circulation in the shallow crust at the EPR axis in the 9° 50'N area.

Acknowledgments. Observations made at the EPR 9° 50'N have been made by many scientists over the last decade, and we thank our colleagues on various Alvin cruises for sharing their ideas and seafloor observations with us. We thank the shipboard and shore based crews of R/V Atlantis and Alvin for their dedication and expertise that resulted in collection of some of the data reported here. The ABE at-sea group—R. Catanach, A. Duester, and A. Billings were instrumental to the success of our 2001 and 2002 data collection efforts, and we thank them for their significant contribution to the acquisition of these important data and the key role they have played in developing the ABE vehicle. Paul Johnson, Akel Sterling and Jenny Engels helped process the DSL-120A sonar data. Dave Dubois helped produce some of the sonar maps. We thank C. Devey, J. Escartin, C. German, D. Naar and W. Wilcock for very constructive reviews that improved the paper. Aerial photographs used in Plate 4 were provided by the U.S. Geological Survey—Hawaii Volcano Observatory. Frank Trusdell of USGS-HVO kindly provided insight and photographs of drainback features on Kilauea volcano. Paul Oberlander helped prepare some of the plates, most notably Plate 12, and his exceptional insight in drawing seafloor perspectives has been very valuable to our research over the years. Field and shore based analyses have been supported by the National Science Foundation under grants OCE-9819261 (H.S. M.A.T and D.J.F.) and OCE-0096468 (D.J.F and T.M.S.), and the Woods Hole Oceanographic Institution's Vetlesen Fund.

REFERENCES

- Alt, J. C., Subseafloor processes in Mid-Ocean Ridge hydrothermal systems, In: *Physical, Chemical, Biological, and Geological Interactions within Seafloor Hydrothermal Systems* (Humphris, S.E., R.A. Zierenberg, L. Mullineaux and R. Thomson). *American Geophysical Union Monograph* 91, 85–114, 1995.
- Ballard, R. D., Holcomb, R. T., and van Andel, T. H., The Galapagos Rift at 86°W: 3. Sheet flows, collapse pits, and lava lakes of the rift valley, *J. Geophys. Res.*, 84, 5407–5422, 1979.
- Barker, D. H. N., G. L. Christenson, J. A. Austin, and I. W. D. Daiziel, Backarc basin evolution and cordilleran orogenesis: Insights from new ocean-bottom seismograph refraction profiling in Bransfield Strait, Antarctica, *Geology*, 31 (2), 107–110, 2003.
- Bazin, S., H. van Avendonk, A. J. Harding, J. A. Orcutt, J. P. Canales, and R.S. Detrick, Crustal structure of the flanks of the East Pacific Rise; implications for overlapping spreading centers, *Geophys. Res. Lett.*, 25, 2213–2216, 1998.
- Begnaud, M. L., J. S. McClain, G. A. Barth, J. A. Orcutt, and A. J. Harding, Velocity structure from forward modeling of the eastern ridge-transform intersection area of the Clipperton fracture zone, East Pacific Rise, *J. Geophys. Res.*, 102, 7803–7820, 1997.

- Bohnenstiehl, D. R. and M. C. Kleinrock, Fissuring near the TAG active hydrothermal mound 26°N on the Mid-Atlantic Ridge, *J. Vol. Geo. Res.*, 98, 33–48, 2000.
- Bohnenstiehl, D. R. and M. C. Kleinrock, Faulting and fault scaling on the median valley floor of the TAG segment, 26°N, Mid-Atlantic Ridge, *J. Geophys. Res.*, 104, 29,351–29,364, 1999.
- Bruce, P. M., and H. E. Huppert, Thermal control of basaltic fissure eruptions, *Nature*, 342, 665–667, 1989.
- Byrnes, J. M., and D. A. Crown, Relationships between pahoehoe surface units, topography, and lava tubes at Mauna Ulu, Kilauea Volcano, Hawaii, *J. Geophys. Res.* 106, 2139–2151, 2001.
- Carbotte, S., and K. C. Macdonald, East Pacific Rise 8 degrees–10 degrees 30'N; evolution of ridge segments and discontinuities from SeaMarc II and three-dimensional magnetic studies, *J. Geophys. Res.*, 97, 6959–6982, 1992.
- Carbotte, S. M., W. B. F. Ryan, M. Cormier, W. Jin, E. Bergmanis, J. Sinton, and S. White, Magmatic subsidence of the EPR 18°14'S revealed through fault restoration of ridge crest bathymetry, *Geochemistry, Geophysics, Geosystems*, 4, 10.1029/2002GC000337, 2003.
- Carbotte, S. M. and D. Scheirer, Variability of ocean crustal structure created along the global midocean ridge, in: *Hydrogeology of Oceanic Lithosphere*, eds.: E. Davis and H. Elderfield, Cambridge University Press, 2003. Cashman, K. V., C. Thornber, and J. P. Kauahikaua, Cooling and crystallization of lava in open channels, and the transition of Pahoehoe Lava to 'A'a, *Bull. Volcanol.*, 61, 306–323, 1999.
- Chadwick, W. W., Jr., T. K. P. Gregg, and R. W. Embley, Submarine lineated sheet flows: a unique lava morphology formed on subsiding lava ponds, *Bull. Volcanol.*, 61, 194–206, 1999.
- Chadwick, Jr., W. W., Quantitative constraints on the growth of submarine lava pillars from a monitoring instrument that was caught in a lava flow, *J. Geophys. Res.*, 108 (B11), 2534, 2003.
- Chadwick, W. W., Jr., D. S. Scheirer, R. W. Embley, and H. P. Johnson, High-resolution bathymetric surveys using scanning sonars: Lava flow morphology, hydrothermal vent and geologic structure at recent eruption sites on the Juan de Fuca Ridge, *J. Geophys. Res.*, 106, 16075–16100, 2001.
- Christeson, G. L., G. M. Kent, G. M. Purdy and R. S. Detrick, Extrusive thickness variability at the East Pacific Rise, 9°–10°N: Constraints from seismic techniques, *J. Geophys. Res.* 101, 2859–2873, 1996.
- Cochran, J. R., D. J. Fornari, B. J. Coakley, R. Herr, and M. A. Tivey, Continuous near-bottom gravity measurements made with a BGM-3 gravimeter in DSV Alvin on the East Pacific Rise crest near 9°30'N and 9°50'N, *J. Geophys. Res.*, 104, 10841–10861, 1999.
- Cormier, M.-H., Ryan, W. B. F., Shah, A. K., Jin, W., Bradley, A. M, and D. R. Yoerger, Waxing and waning volcanism along the East Pacific Rise on the millennium time scale, *Geology*, 31, 633–636, 2003.
- Crawford, W. C., and S. C. Webb, Variations in the distribution of magma in the lower crust and at the Moho beneath the East Pacific Rise at 9°–10°N, *Earth and Planet. Sci. Lett.*, 203, 117–130, 2002.
- Crawford, W. C., S. C. Webb, and J. A. Hildebrand, Constraints on melt in the lower crustal and Moho at the East Pacific Rise, 9 degrees 48'N, using seafloor compliance measurements, *Journal of Geophysical Research, B, Solid Earth and Planets*, 104 (2), 2923–2939, 1999.
- Crown, D. A., and S. M. Baloga, Pahoehoe toe dimensions, morphology, and branching relationships at Mauna Ulu, Kilauea Volcano, Hawaii, *Bull. Volcanol.*, 61, 288–305, 1999.
- Curwitz, D. and J. A. Karson, Geological consequences of dike intrusion at Mid-Ocean Ridge spreading centers, in: Faulting and magmatism at mid-ocean ridges, W. R. Buck, et al. (eds.), *Am. Geophys. U. Geophys. Monograph* 106, 117–136, 1998.
- Delaney, J. R., D. S. Kelley, M. D. Lilley, D. A. Butterfield, J. A. Baross, W. S. D. Wilcock, R. W. Embley and M. Summit, The quantum event of oceanic crustal accretion: Impacts of diking at mid-ocean ridges. *Science* 281: 222–230, 1998.
- Delaney, J. R., V. Robigou, R. McDuff, and M. Tivey, Geology of Vigorous Hydrothermal System on the Endeavour Segment, Juan de Fuca Ridge, *J. Geophys. Res.*, 97, 19,663–19,682, 1992.
- Delaney, P. T., and D. D. Pollard, Solidification of basaltic magma during flow in a dike, *Am. J. Sci.*, 282, 856–885, 1982.
- Detrick, R. S., P. Buhl, E. E. Vera, J. C. Mutter, J. A. Orcutt, J. A. Madson, and T. M. Brocher, Multi-channel seismic imaging of a crustal magma chamber along the East Pacific Rise, *Nature*, 326 (6108), 35–41, 1987.
- Dunn, R. A., and D. R. Toomey, Seismological evidence for three-dimensional melt migration beneath the East Pacific Rise, *Nature*, 388, 259–262, 1997.
- Eaton, J. P., D. H. Richter, and H. L. Krivoy, *Cycling of Magma Between the Summit Reservoir and Kilauea Iki Lava Lake During the 1959 Eruption of Kilauea Volcano*, 1307–1335 pp., USGS Prof. Paper, 1987.
- Embley, R. W., and W. W. Chadwick, Jr., Volcanic and hydrothermal processes associated with a recent phase of seafloor spreading at the northern Cleft segment: Juan de Fuca Ridge, *J. Geophys. Res.*, 99, 4741–4760, 1994.
- Embley, R. W., Chadwick, W. W., Jonasson, I. R., Butterfield, D. A., and E. T. Baker, Initial results of the rapid response to the 1993 CoAxial event: Relationships between hydrothermal and volcanic processes, *Geophys. Res. Letts.*, 22, 143–146, 1995.
- Embley, R. W., Chadwick, W.W., Clague, D. and D. Stakes, 1998 eruption of Axial volcano: Multibeam anomalies and seafloor observations, *Geophys. Res. Lett.*, 26, 3425–3428, 1999.
- Embley, R. W., Chadwick, W. W., Perfit, M. R., Smith, M. C. and J.R. Delaney, Recent eruptions on the CoAxial segment of the Juan de Fuca Ridge: Implications for mid-ocean ridge accretion processes, *J. Geophys. Res.*, 105, 16,501–16,525, 2000.
- Embley, R. W. et al., Rediscovery and exploration of Magic Mountain, Explorer Ridge, NE Pacific, *Eos Trans. AGU*, 83(47), Fall Meet. Suppl., Abstract T11C–1264, 2002.
- Embley, R. W. and E. Baker, 2003.
- Engels, J. L., M. H. Edwards, D. J. Fornari, M. R. Perfit, G. J. Kurras, D. R. Bohnenstiehl, A new model for submarine volcanic collapse formation, *G³*, 2003
- Fink, J. H., and R. W. Griffiths, A laboratory analog study of the surface morphology of lava flows extruded from point and line sources, *Journal of Volcanology and Geothermal Research*, 54, 19–32, 1992.

- Fornari, Escartin et al. AST paper in prep
- Fornari, D. J., Van Dover, C. L., Shank, T., Lutz, R. and M. Olsson, A versatile, low-cost temperature sensing device for time-series measurements at deep sea hydrothermal vents, *BRIDGE Newsletter*, 6, 37–40, 1994.
- Fornari, D. J., and Embley, R. W, Tectonic and volcanic controls on hydrothermal processes at the Mid-Ocean Ridge: An overview based on near-bottom and submersible studies. In: *Physical, Chemical, Biological, and Geological Interactions within Seafloor Hydrothermal Systems* (Humphris, S. E., R. A. Zierenberg, L. Mullineaux and R. Thomson). *American Geophysical Union Monograph 91*, 1–46, 1995.
- Fornari, D. J., F. Voegeli, and M. Olsson, Improved low-cost, time-lapse temperature loggers for deep ocean and sea floor observatory monitoring, *RIDGE Events*, 7, 13–16, 1996.
- Fornari, D. J., Haymon, R. M., Perfit, M. R., Gregg, T. K. P., Edwards, M. H., Geological Characteristics and Evolution of the Axial Zone on Fast Spreading Mid-Ocean Ridges: Formation of an Axial Summit Trough along the East Pacific Rise, 9°–10°N, *J. Geophys. Res.*, 103, 9827–9855, 1998a.
- Fornari, D. J., T. Shank, K. L. Von Damm, T. K. P. Gregg, M. Lilley, G. Levai, A. Bray, R. M. Haymon, M. R. Perfit and R. Lutz, Time-Series Temperature Measurements at High-Temperature Hydrothermal Vents, East Pacific Rise 9° 49'–51'N: Monitoring a Crustal Cracking Event, *Earth Planet. Sci. Lett.*, 160, 419–431, 1998b.
- Fornari, D. J. and T. M. Shank, Summary of High- and Low-T Tiime Series Vent Fluid Temperature Experiments East Pacific Rise 9° 49'–51'N, EXTREME-1 Cruise - May 1999, R/V Atlantis 03–34, Cruise Report, July 1, 1999.
- Fornari, D. J., M. Perfit, M. Tolstoy, D. Scheirer and Science Party, *AHA-Nemo2 Cruise Report* cruise data web site: <http://science.who.edu/ahanemo2>, 2001.
- Fornari, D. J., A new deep-sea towed digital camera and multi-rock coring system, *EOS*, 84, 69&73, 2003.
- Fornari, D. J. M. Tivey, H. Schouten, D. Yoerger, A. Bradley, M. R. Perfit, D. Scheirer, P. Johnson, M. H. Edwards, R. Haymon, S. Humphris, DSL-120A High-Resolution, Near-Bottom Sidescan Sonar Imaging of Mid-Ocean Ridge Crests: East Pacific Rise, Galapagos Rift and Mid-Atlantic Ridge, *EGS/AGU/EUG Joint Meeting*, Nice, France, abstract EAE03-A-02862, 2003a.
- Fornari, D. J. Gray, R., Olsson, M., Shank, T., and K. Von Damm, High-T Hydrothermal Vent Monitoring at the East Pacific Rise 9°50'N and a New, Improved 64k Memory High-T Vent Fluid Temperature Logger, *Ridge2000 Events*, 21–25, 2003b.
- Fox, C. G., Chadwick, W. W. and Embley, R. W., Direct observation of a submarine volcanic eruption from a sea-floor instrument caught in a lava flow. *Nature*, 412: 727–729, 2001.
- Fox, C. G., W. E. Radford, R. P. Dziak, T. K. Lau, H. Matsumoto, and A. E. Schreiner, Acoustic detection of a seafloor spreading episode on the Juan de Fuca Ridge using military hydrophone arrays, *Geophys. Res. Letts.*, 22, 131–134, 1995.
- Francheteau, J. and R. D. Ballard, The East Pacific Rise near 21°N, 13°N and 20°S: Inferences for along-strike variability of axial processes of the mid-ocean ridge, *Earth Planet. Sci. Lett.*, 64, 93–116, 1983.
- Garmany, J., Accumulations of melt at the base of young oceanic crust, *Nature*, 340, 628–632, 1989.
- German, C. R. & K. L. Von Damm, Chapter 6.10 Hydrothermal Processes, in *The Treatise of Geochemistry*, eds. K. K. Turekian & H. D. Holland, *Elsevier*, pp. 181–222, 2004
- Germanovich, L. N., R. P. Lowell, and D. K. Astakhov, Temperature-dependent permeability and bifurcations in hydrothermal flow, *J. Geophys. Res.*, 106, 473–495, 2001.
- Greenland, L. P., Okamura, A. T. and J. B. Stokes, 5. Constraints on the mechanics of the eruption, in: *The Puu OO eruption of Kilauea volcano, Hawaii: Episodes 1 Through 20, January 3, 1983, Through June 8, 1984*, ed. E. Wolfe, *US Geol. Survey Prof. Paper 1463*, US Government Printing Office, Washington, DC, 1988.
- Gregg, T. K. P., D. J. Fornari, M. R. Perfit, W. I. Ridley and M. D. Kurz, Using submarine lava pillars to record mid-ocean ridge eruption dynamics, *Earth Planet. Sci. Lett.*, 178, 195–214, 2000.
- Gregg, T. K., and D. J. Fornari, Long submarine lava flows: observations and results from numerical modeling, *Journal of Geophysical Research*, 103 (B11), 27517–27531, 1998.
- Gregg, T. K. P., Fink, Jonathan H., Griffiths, Ross W., Formulation of multiple fold generations on lava flow surfaces: influence of strain rate, cooling rate, and lava composition, *Journal of Volcanology and Geothermal Research*, 80, 281–292, 1998.
- Gregg, T. K. P., Fornari, D. J., Perfit, M. R., Haymon, R.M., and Fink, J. H., Rapid Emplacement of a Mid-Ocean Ridge Lava Flow: The East Pacific Rise at 9° 46'–51'N, *Earth Planet. Sci. Express Lett.*, 144:, E1–E7, 1996.
- Griffiths, R. W. a. F., Jonathan H., The morphology of lava flows in planetary environments: predictions from analog experiments, *Journal of Geophysical Research*, 97 (B13), 19,739–19,748, 1992.
- Hannington, M. D., Jonasson, I. R., Herzig, P. M., and S. Petersen, Physical and chemical processes of seafloor mineralization at Mid-Ocean Ridges, In: *Physical, Chemical, Biological, and Geological Interactions within Seafloor Hydrothermal Systems* (Humphris, S. E., R. A. Zierenberg, L. Mullineaux and R. Thomson). *American Geophysical Union Monograph 91*, 115–157, 1995.
- Harding, A. J., G. M. Kent, and J. A. Orcutt, A multichannel seismic investigation of upper crustal structure at 9 degrees N on the East Pacific Rise; implications for crustal accretion, *J. Geophys. Res.*, 98, 13,925–13,944, 1993.
- Haymon, R. M., and S. M. White, Fine-scale segmentation of volcanic/hydrothermal systems along fast-spreading ridge crests, *Earth Planet. Sci. Lett.*, in press.
- Haymon, R. M., The response of ridge-crest hydrothermal systems to segmented, episodic magma supply, in: *Tectonic, Magmatic, Hydrothermal and Biological Segmentation of Mid-Ocean Ridges*, eds: C. J. MacLeod, P. A. Tyler and C. L. Walker, *Geol. Soc. Spec. Publ.*, 118, 157–168. 1996.
- Haymon, R. M., D. J. Fornari, K. L. Von Damm, M. D. Lilley, M. R. Perfit, and J. M. Edmond, Volcanic eruption of the mid-ocean ridge along the East Pacific Rise crest at 9 degree 45–52'N: Direct submersible observations of seafloor phenomena associated with an eruption event in April, 1991. *Earth Planet. Sci. Lett.*, 119, 85–101, 1993.

- Haymon, R. M., D. J. Fornari, M. H. Edwards, S. Carbotte, D. Wright and K. C. Macdonald, Hydrothermal vent distribution along the East Pacific Rise crest (9°09'–54'N) and its relationship to magmatic and tectonic processes on fast-spreading mid-ocean ridges, *Earth Planet. Sci. Lett.*, 104, 513–534, 1991.
- Heliker, C. C., M. T. Mangan, T. N. Mattox, J. P. Kauahikaua, and R. T. Helz, The character of long-term eruptions: inferences from episodes 50–53 of the Pu'ū 'Ō'o-Kupaianaha eruption of Kilauea Volcano, *Bull. Volcanol.* 59, 381–393, 1998.
- Herron, T. J., P. L. Stoffa, and P. Buhl, Magma chamber and mantle reflections; East Pacific Rise, *Geophysical Research Letters*, 7 (11), 989–992, 1980.
- Holcomb, R. T., Eruptive history and long-term behavior of Kilauea Volcano, in *U.S. Geological Survey Professional Paper 1350*, edited by R. W. Decker, T. L. Wright, and P. H. Stauffer, pp. 261–350, 1987.
- Holcomb, R. T., Preliminary geologic map of Kilauea Volcano, Hawaii, *U.S. Geological Survey*, 80–796, 1980.
- Hon, K., J. Kauahikaua, R. Denlinger, and K. Mackay, Emplacement and inflation of pahoehoe sheet flows: observations and measurements of active lava flows on Kilauea Volcano, Hawaii, *Geological Society of America Bulletin*, v. 106, p. 351–370, 1994.
- Humphris, S. E., Hydrothermal processes at mid-ocean ridges, *U.S. Natl. Rep. Int. Union Geod. Geophys. 1991–1994, Rev. Geophys.*, 33, 71–80, 1995.
- Jakuba, M., D. Yoerger, W. Chadwick, A. Bradley, R. Embley, Multi-beam sonar mapping of the Explorer Ridge with an Autonomous Underwater Vehicle *Eos Trans. AGU*, 83(47), Fall Meet. Suppl., Abstract T11C-1266, 2002.
- Johnson, H. P., S. L. Hautala, M. A. Tivey, C. D. Jones, J. Voight, M. Pruis, I. Garcia-Berdeal, L. A. Gilbert, T. Bjorklund, W. Fredericks, J. Howland, M. Tsurumi, T. Kurokawa, K. Nakamura, K. O'Connell, L. Thomas, S. Bolton, and J. Turner, Survey studies hydrothermal circulation on the northern Juan de Fuca Ridge, *EOS*, 83, 73–79, 2002.
- Kent, G. M., A. J. Harding, and J. A. Orcutt, Evidence for a smaller magma chamber beneath the East Pacific Rise at 9°30'N, *Nature*, 412, 145–149, 1990.
- Kent, G. M., A. J. Harding, and J. A. Orcutt, Distribution of magma beneath the East Pacific Rise between the Clipperton Transform and the 9 degrees 17'N Deval from forward modeling of common depth point data, *J. Geophys. Res.*, 98, 13,945–13,969, 1993a.
- Kent, G. M., A. J. Harding, and J. A. Orcutt, Distribution of magma beneath the East Pacific Rise near the 9 degrees 03'N overlapping spreading center from forward modeling of common depth point data, *J. Geophys. Res.*, 98, 13,971–13,995, 1993b.
- Kilburn, C. R. J., Patterns and predictability in the emplacement of subaerial lava flows and flow fields, in *Monitoring and mitigation of volcano hazards*, edited by R. Scarpa, and R. I. Tilling, pp. 491–537, Springer-Verlag, Berlin, 1996.
- Kurokawa, T., M. H. Edwards, P. Johnson, D. J. Fornari, M. Perfit, H. Schouten, and M. A. Tivey, Possible Recent Volcanic Activity on the East Pacific Rise at 9° 32'N, *Eos Trans. AGU*, 83(47), Fall Meet. Suppl., Abstract V52A-1283, 2002.
- Kurras, G., D. J. Fornari and M. H. Edwards, Volcanic morphology of the East Pacific Rise crest 9°49'–52'N: Implications for extrusion at fast spreading mid-ocean ridges, *Mar. Geophys. Res.*, 21, 23–41, 2000.
- Lerner, S., D. Yoerger and T. Crook, Navigation for the Derbyshier Phase2 Survey, *Woods Hole Oceanographic Institution Technical Report*, 24 pp., May, 1999.
- Lilley, M. D., Butterfield, D. A., Lupton, J. E., and E. J. Olson, Magmatic events can produce rapid changes in hydrothermal vent chemistry, *Nature*, 422, 878–881, 2003
- Lowell, R. P. and L. N. Germanovich, On the temporal evolution of high-temperature hydrothermal systems at ocean ridge crests, *J. Geophys. Res.*, 99, 565–575, 1994.
- Lupton, J. E., E. T. Baker, M. J. Mottl, F. J. Sansone, C. G. Wheat, J. A. Resing, G. J. Massoth, C. I. Measures, and R. A. Feely, Chemical and physical diversity of hydrothermal plumes along the East Pacific Rise, 8°45'N to 11°50'N, *Geophysical Research Letters*, 20, 2913–2916, 1993.
- Lutz, R. A., T. M. Shank, D. J. Fornari, R. M. Haymon, M. D. Lilley, K. L. Von Damm & D. Desbruyeres, Rapid growth at deep-sea vents, *Nature*, 371, 663–664, 1994.
- Macdonald, K., J.-C. Sempere, and P. J. Fox, East Pacific Rise from Siqueiros to Orozco fracture zones; along-strike continuity of axial neovolcanic zone and structure and evolution of overlapping spreading centers, *J. Geophys. Res.* 89, 6049–6069, 1984.
- Macdonald, K. C., P. J. Fox, S. Miller, S. Carbotte, M. H. Edwards, M. Eisen, D. J. Fornari, L. Perram, R. Pockalny, D. Scheirer, S. Tighe, C. Weiland and D. Wilson, The East Pacific Rise and its flanks 8–18°N: History of segmentation, propagation and spreading direction based on SeaMARC II and Sea Beam studies, *Mar. Geophys. Res.*, 14, 299–344, 1992.
- Mattox, T., C. Heliker, J. Kauahikaua, and K. Hon, Development of the 1990 Kalapana flow field, Kilauea Volcano, Hawaii, *Bulletin of Volcanology*, 55 (407–413), 1993.
- McClain, J. S., Begnaud, M. L., Wright, M. A., Fondrk, J. and K. Von Damm, Seismicity and tremore in a submarine hydrothermal field: the northern Juan de Fuca Ridge, *Geophys. Res. Lett.*, 20, 1883–1886, 1993.
- Morton, J. L., M. L. Holmes, and R. A. Koski, Volcanism and massive sulfide formation at a sedimented spreading center, Escanaba Trough, Gorda Ridge, northeast Pacific Ocean, *Geophys. Res. Letts.*, 14, 769–772, 1987.
- Mullineaux, L. S., S. W. Mills and E. Goldman, Recruitment variation during a pilot colonization study of hydrothermal vents (9°50'N, East Pacific Rise). *Deep-Sea Res. II* 45: 441–464, 1998.
- Naar, D. F. and R. N. Hey, Recent Pacific-Easter-Nazca plate motions, in: *Evolution of Mid-Ocean Ridges*, *Geophys. Monogr. Ser.*, 57, ed. J. Sinton, 9–30, AGU, Washington, DC., 1989.
- Oosting, S. E. and K. L. von Damm, Bromide/chloride fractionation in seafloor hydrothermal fluids from 9–10°N East Pacific Rise, *Earth Planet. Sci. Lett.*, 144, 133–145, 1996.
- Parfitt, E. A., T. K. P. Gregg, and D. K. Smith, A comparison between subaerial and submarine eruptions at Kilauea Volcano, Hawaii: implications for the thermal viability of lateral feeder dikes, *J. Volcanol. Geotherm. Res.*, 113, 213–242, 2002.

- Parfitt, E. A., and L. Wilson, The 1983–86 Pu‘u ‘O‘o eruption of Kilauea Volcano, Hawaii; a study of dike geometry and eruption mechanisms for a long-lived eruption, *J. Volcanol. Geotherm. Res.*, 59, 179–205, 1994.
- Perfit, M. R., J. R. Cann, D. J. Fornari et al., Interaction of seawater and lava during submarine eruptions at mid-ocean ridges, 2003 nature paper
- Perfit, M. R. and W. C. Chadwick, Magmatism at mid-ocean ridges: Constraints from volcanological and geochemical investigations, in: Faulting and magmatism at mid-ocean ridges, W.R. Buck, et al. (eds.), *Am. Geophys. U. Geophys. Monograph* 106, 59–116, 1998.
- Perfit, M. R., Fornari, D. J., Smith, M., Bender, J., Langmuir, C. H., Haymon, R. M., Across-axis spatial and temporal diversity of MORB on the crest of the East Pacific Rise between 9°30′–9°32′N, *Geology*, 22, 375–379, 1994.
- Pockalny, R. A., P. J. Fox, D. J. Fornari, K. C. Macdonald, and M. R. Perfit, Tectonic reconstruction of the Clipperton and Siqueiros Fracture zones: Evidence and consequences of plate motion change for the last 3 Myr, *J. Geophys. Res.*, 102, 3167–3182, 1997.
- Polacci, M., K. V. Cashman, and J. P. Kauahikaua, Textural characterization of the pahoehoe – ‘a’ transition in Hawaiian basalt, *Bull. Volcan.*, 60, 595–609, 1999.
- Ravizza, G., J. Blusztain, K. L. Von Damm, A. M. Bray, W. Bach, and S. R. Hart, Sr isotope variations in vent fluids from 9° 46′–9°54′N East Pacific Rise: evidence of a non-zero Mg fluid component, *Geochem. Cosmochem. Acta*, 65, 729–739, 2001.
- Rohr, K. M., Increase of seismic velocities in upper oceanic crust and hydrothermal circulation in the Juan de Fuca plate, *Geophys. Res. Lett.*, 21, 2163–2166, 1994.
- Rubin, K. H., J. D. MacDougall, and M. R. Perfit, $^{210}\text{Po}/^{210}\text{Pb}$ dating of recent volcanic eruptions on the sea floor, *Nature*, 468, 841–844, 1994.
- Sakimoto, S. E. H. and Gregg, T. K. P., Channeled flow: Analytic solutions, laboratory experiments, and applications to lava flows. *J. Geophys. Res.*, 106(5): 8629–8644, 2001.
- Scheirer, D. S., D. J. Fornari, S. E. Humphris, and S. Lerner, High-Resolution Seafloor Mapping Using the DSL-120 Sonar System: Quantitative Assessment of Sidescan and Phase-Bathymetry Data from the Lucky Strike Segment of the Mid-Atlantic Ridge, *Mar. Geophys. Res.* 21, 121–142, 2000.
- Scheirer, D. S., and K. C. Macdonald, Variation in cross-sectional area of the axial ridge along the East Pacific Rise; evidence for the magmatic budget of a fast spreading center, *J. Geophys. Res.*, 98, 7871–7885, 1993.
- Scheirer, D. S., T. M. Shank, and D. J. Fornari, Temperature variations at diffuse-flow hydrothermal vent sites along the East Pacific Rise, *Earth Planet. Sci. Lett.*, (submitted).
- Schouten, H., M. A. Tivey, D. J. Fornari, and J. R. Cochran, Central Anomaly Magnetization High: Constraints on the volcanic construction and architecture of seismic layer 2A at a fast-spreading Mid-Ocean Ridge, the EPR at 9°30′–50′N, *Earth Planet. Sci. Lett.*, 169, 37–50, 1999.
- Schouten, H., Tivey, M. A., and D. J. Fornari, *AT7-4 Cruise Report*, at: <http://imina.soest.hawaii.edu/HMRG/EPR/index.htm> under AT7-4 Cruise Report, 2001.
- Schouten, H., M. Tivey, D. Fornari, D. Yoerger, A. Bradley, P. Johnson, M. Edwards, and T. Kurokawa, Lava Transport and Accumulation Processes on EPR 9 27′N to 10N: Interpretations Based on Recent Near-Bottom Sonar Imaging and Seafloor Observations Using ABE, Alvin and a new Digital Deep Sea Camera, *Eos Trans. AGU*, 83(47), Fall Meet. Suppl., Abstract T11C-1262, 2002.
- Shank, T. S., D. J. Fornari, and R. Lutz, Periodicities and variability of high and low-temperature hydrothermal venting along the Bio-transect (9° 50′N) on the East Pacific Rise: three years of continuous synchronous temperature monitoring, *Eos, Trans. Amer. Geophys. Union*, 78, F739, 1997.
- Shank, T. M., D. J. Fornari, K. L. Von Damm, M. D. Lilley, R. M. Haymon and R. A. Lutz, Temporal and spatial patterns of biological community development at nascent deep-sea hydrothermal vents along the East Pacific Rise, *Deep Sea Res. II* 45, 465–515, 1998.
- Shank, T. M., Hammond, S., D. J. Fornari, et al., Time-Series Exploration and Biological, Geological, and Geochemical Characterization of the Rosebud and Calyfield Hydrothermal Vent Fields at 86°W and 89.5°W on the Galapagos Rift, *Eos*, T11C-1257, 2002.
- Shank, T. M., D. S., Scheirer, and D. J. Fornari, Influences of temperature and chemistry on habitat selection at hydrothermal vents, *Limnology and Oceanography*, (submitted).
- Singh, S. C., G. M. Kent, J. S. Collier, A. J. Harding, and J. A. Orcutt, Melt to mush variations in crustal magma properties along the ridge crest at the southern East Pacific Rise, *Nature (London)*, 394 (6696), 874–878, 1998.
- Sinton, J., Bergmanis, E., Rubin, K. et al., volcanic eruptions on mid-ocean ridges: New evidence from the superfast spreading East Pacific Rise, 17°–19°S, *J. Geophys. Res.*, 107, 10.1029/2000JB000090, 2002.
- Sinton, J. M., and R. S. Detrick, Mid-ocean ridge magma chambers, *J. Geophys. Res.*, 97, 197–216, 1992.
- Smith, M., M. R. Perfit, D. J. Fornari, W. Ridley, I., M. H. Edwards, G. Kurras, and K. L. Von Damm, Segmentation and Magmatic Processes at a Fast Spreading Mid-Ocean Ridge: Detailed Geochemistry and Mapping of the East Pacific Rise Crest at the 9° 37′N OSC, *G³*, 2, paper #2000GC000134, 2001.
- Sohn R., D. J. Fornari, K. L. Von Damm, S. Webb, and J. Hildebrand, Seismic and hydrothermal evidence for a propagating cracking event on the East Pacific Rise crest at 9° 50′N, *Nature*, 396, 159–161, 1998.
- Sohn, R. A., J. A. Hildebrand, and S. C. Webb, A microearthquake survey of the high-temperature vent fields on the volcanically active East Pacific Rise, *J. Geophys. Res.*, 104 (11), 25,367–25,378, 1999.
- Soule, S. A., K. V. Cashman, and J. P. Kauahikaua, Examining flow emplacement through the surface morphology of three rapidly emplaced, solidified lava flows, Kilauea Volcano, Hawai‘I, *Bull. Volcanology*, 66, 1–14, 2004.

- Stewart, W. K., Chu, D., Malik, S., Lerner, S., and H. Singh, Quantitative seafloor characterization using a bathymetric sidescan sonar, *J. Ocean. Engin.* 19, 599–610, 1994.
- Swanson, D. A., Pahoehoe flows from the 1969–1971 Mauna Ulu eruption, Kilauea Volcano, Hawaii, *Geological Society of America Bulletin*, v. 84, p. 615–626, 1973.
- Tian, T., W. S. D. Wilcock, D. R. Toomey, and R. S. Detrick, Seismic heterogeneity in the upper crust near the 1991 eruption site on the East Pacific Rise, 9 degrees 50'N, *Geophysical Research Letters*, 27 (16), 2369–2372, 2000.
- Tilling, R. I., Christiansen, R. L., Duffield, W. A. et al., The 1972–1974 Maunu Ulu eruption, Kilauea volcano: an example of quasi-steady state magma transfer, in: Decker, R. W, Wight, T. L. and P. H. Stauffer, eds., *USGS Prof. Paper 1350*, 405–469.
- Tivey, M., D. Fornari, H. Schouten, D. Yoerger, A. Bradley, P. Johnson, R. Embley, High-Resolution Magnetic Field and Bathymetric Imaging of Hydrothermal Vent Areas using Autonomous Underwater Vehicles, Remotely Operated Vehicles and Submersibles, EGS/AGU/EUG Joint Meeting, Nice, France, abstract EAE03-A-02858, 2003.
- Tivey, M. A. and H. P. Johnson, Crustal magnetization reveals subsurface structure of Juan de Fuca Ridge hydrothermal fields, *Geology*, 30, 979–982, 2002.
- Tivey, M. A., H. P. Johnson, A. Bradley, and D. Yoerger, Thickness measurements of submarine lava flows determined from near-bottom magnetic field mapping by autonomous underwater vehicle, *Geophys. Res. Lett.*, 25, 805–808, 1998.
- Tivey, M. A., A. Bradley, D. Yoerger, R. Catanach, A. Dueter, S. Liberatore and H. Singh, Autonomous underwater vehicle maps seafloor, *EOS*, 78, 229–230, 1997(a).
- Tivey, M. A., A. Bradley, D. Yoerger, R. Catanach, A. Dueter, S. Liberatore and H. Singh, Autonomous underwater vehicle maps seafloor, *Earth in Space*, 10, 10–14, 1997(b).
- Toomey, D. R., G. M. Purdy, S. C. Solomon, and W. S. D. Wilcock, The three-dimensional seismic velocity structure of the East Pacific Rise near latitude 9 degrees 30' N, *Nature*, 347 (6294), 639–645, 1990.
- Toomey, D. R., S. C. Solomon, and G. M. Purdy, Tomographic imaging of the shallow crustal structure of the East Pacific Rise at 9°30'N, *J. Geophys. Res.* 99, 24,135–24,157, 1994.
- Umino, S., Obata, S., Lipman, P., et al., Emplacement and inflation structures of submarine and subaerial pahoehoe lavas from Hawaii. Hawaiian Volcanoes: Deep Underwater perspectives, *American Geophys. Mono.* 128, 85–102, 2002.
- van Avendonk, H. J. A., A. J. Harding, and J. A. Orcutt, Contrast in crustal structure across the Clipperton transform fault from travel time tomography, *J. Geophys. Res.* B, 106, 10,961–10,981, 2001.
- van Avendonk, H. J. A., A. J. Harding, J. A. Orcutt, and J. S. McClain, A two-dimensional tomographic study of the Clipperton transform fault, *J. Geophys. Res.*, 103, 17,885–17,899, 1998.
- van Dover, C. L., S. E. Humphris, D. Fornari, C. M. Cavanaugh, R. Collier, S. K. Goffredi, J. Hashimoto, M. Lilley, A.-L. Reysenbach, T. Shank, K. L. Von Damm, A. Banta, R. M. Gallant, D. Gotz, D. Green, J. Hall, T. L. Harmer, L. A. Hurtado, P. Johnson, Z. P. McKiness, C. Meredith, E. Olson, I. L. Pan, M. Turnipseed, Y. Won, C. R. Young III, and R. C. Vrijenhoek, Biogeography and Ecological Setting of Indian Ocean Hydrothermal Vents, *Science*, 294, 818–823, 2001.
- Vera, E. E., and J. B. Diebold, Seismic imaging of oceanic layer 2A between 9°30'N and 10°N on the East Pacific Rise from two-ship wide-aperture profiles, *Journal of Geophysical Research*, 99, 3031–3041, 1994.
- Vera, E. E., J. C. Mutter, P. Buhl, J. A. Orcutt, A. J. Harding, M. E. Kappus, R. S. Detrick, and T. M. Brocher, The structure of 0- to 0.2-m.y.-old oceanic crust at 9 degrees N on the East Pacific Rise from expanded spread profiles, *J. Geophys. Res.*, 95, 15,529–15,556, 1990.
- Vera, E. E., and J. B. Diebold, Seismic imaging of oceanic layer 2A between 9°30'N and 10°N on the East Pacific Rise from two-ship wide-aperture profiles, *Journal of Geophysical Research*, 99, 3031–3041, 1994.
- Von Damm, K. L., Evolution of the Hydrothermal System at East Pacific Rise 9°50'N: Geochemical Evidence for Changes in the Upper Oceanic Crust, in: German, C. R., Lin, J., Parson, L., eds., *AGU Monograph*.
- Von Damm, K. L., Lilley, M. D., Shanks, W. C. III, et al., Extraordinary phase separation and segregation in vent fluids from the Southern East Pacific Rise, *Earth Planet. Sci. Lett.*, 206, 365–378, 2003a.
- Von Damm, K. L., and M. D. Lilley, Diffuse flow hydrothermal fluids from 9°50'N East Pacific Rise: origin, evolution, and biogeochemical controls, in: *The Subsurface Biosphere at Mid-Ocean Ridges*, AGU monograph RIDGE Theoretical Institute), W. Wilcock et al., eds., in press, 2004.
- Von Damm, K. L., Chemistry of hydrothermal vent fluids from 9–10°N, East Pacific Rise: “Time zero” the immediate post-eruptive period, *J. Geophys. Res.* 105, 11203–11222, 2000.
- Von Damm, K. L., Bray, A. M., Buttermore, L. G. Oosting, S.E. The geochemical controls on vent fluids from the Lucky Strike vent field, Mid-Atlantic Ridge, *Earth and Planet. Sci. Lett.*, 160, 521–536, 1998
- Von Damm, K. L., Buttermore L. G., Oosting S. E., Bray A. M., Fornari DJ, Lilley M.D., et al., Direct observation of the evolution of a seafloor ‘black smoker’ from vapor to brine. *Earth Planet. Sci. Lett.*, 149, 101–111, 1997.
- Von Damm, K. L., A. M. Bray, L. G. Buttermore, M. D. Lilley, E. J. Olson and E. McLaughlin, Chemical changes between high temperature and diffuse flow fluids at 9° 50'N East Pacific Rise, *Eos Trans. AGU*, 77 (46), F403–404, 1996.
- Von Damm, K. L., Temporal and compositional diversity in seafloor hydrothermal fluids, *Rev. of Geophys.*, U.S. National Report to International Union of Geodesy and Geophysics, 1297–1305, 1995.
- Von Damm, K. L., S. E. Oosting, R. Kozlowski, L. G. Buttermore, D. C. Colodner, H. N. Edmonds, J. M. Edmond, and J. M. Grebmeier, Evolution of East Pacific Rise hydrothermal vent fluids following a volcanic eruption, *Nature*, 375, 47–50, 1995.
- Von Damm, K. L., Seafloor Hydrothermal Activity: Black Smoker Chemistry and Chimneys, *Annu. Rev. Earth Planet. Sci.*, 18, 173–204, 1990
- Wallace, P. J. and A. T. Anderson, Jr., Effects of eruption and lava drainback on the H2) contents of basaltic magmas at Kilauea Volcano, *Bull. Volcanol.*, 59, 327–344, 1998.

- West, M., Menke, W., Tolstoy, M., Webb, S., and R. Sohn, Magma storage beneath Axial volcano on the Juan de Fuca mid-ocean ridge, *Nature*, 413, 833–836, 2003.
- West, M., W. Menke, M. Tolstoy, S. C. Webb, and R. A. Sohn, Magma storage beneath Axial volcano on the Juan de Fuca mid-ocean ridge, *Nature*, 413, 833–836, 2001.
- White S. M., R. M. Haymon, D. J. Fornari, K. C. Macdonald, and M.R. Perfit, Volcanic Structures and Lava Morphology of the East Pacific Rise, 9°–10°N: Constraints on Volcanic Segmentation and Eruptive Processes at Fast-Spreading Ridges, *J. Geophys. Res.*, 107, 10,1029, 2001JB000571, 2002.
- Wilcock, W. S. D., The physical response of mid-ocean ridge hydrothermal systems to local earthquakes, *Geochemistry, Geophysics, Geosystems*, *In press*, 2004.
- Wilcock, W. S. D., Cellular convection models of mid-ocean ridge hydrothermal circulation and the temperatures of black smoker fluids, *J. Geophys. Res.*, 103, 2585–2596, 1998.
- Wolfe, E. W., Garcia, M. O., Jackson, D. B., et al., The Puu OO eruption of Kilauea volcano, episodes 1–20, January 3, 1983 to June 8, 1984, in: Decker, R. W., Wight, T. L. and P. H. Stauffer, eds., *USGS Prof. Paper 1350*, 471–508, 1987.
- Wolfe, E. W., Neal, C. A., Banks, N. G. and Duggan, T. J., Geologic observations and chronology of eruptive events. In: E. W. Wolfe (Eds.) *USGS Prof. Paper 1463*. The Puu Oo eruption of Kilauea Volcano, Hawaii: Episodes 1 through 20, January 3, 1983, through June 8, 1984, pp. 1–98, 1988.
- Wright, D. J., Haymon, R. M., and D. J. Fornari, Crustal fissuring and its relationship to magmatic and hydrothermal processes on the East Pacific Rise crest (9°12′–54′N), *J. Geophys. Res.*, 100, 6097–6120, 1995a.
- Wright, D. J., Haymon, R. M., and K. C. Macdonald, Breaking new ground: Estimates of crack depth along the axial zone of the East Pacific Rise (9° 12′–54′N), *Earth Planet. Sci. Lett.*, 134, 441–457, 1995b.
- Wright, D. J., Formation and development of fissures at the East Pacific Rise: Implications for faulting and magmatism at Mid-Ocean ridges, in: Faulting and magmatism at mid-ocean ridges, W.R. Buck, et al. (eds.), *Am. Geophys. U. Geophys. Monograph 106*, 137–151, 1998.
- Wright, D. J., R. M. Haymon, S. M. White, and K. C. Macdonald, Crustal fissuring on the crest of the southern East Pacific Rise at 17° 15′–40′S, *J. Geophys. Res.*, 107, 10,1029/2001JB000544, 2002.
- Wylie, J. J., K. R. Helfrich, B. Dade, J. R. Lister, and J. F. Salzig, Flow localization in fissure eruptions, *Bull. Volcanol.*, 60, 432–440, 1999.
- Yang, J. K. Latychev, and R. N. Edwards, Numerical computation of hydrothermal fluid circulation in fractured Earth structures, *Geophys. J. Int.*, 135, 627–649, 1998.
- Yoerger, D., A. Bradley, R. Bachmayer, R. Catanach, A. Duester, S. Liberatore, H. Singh, B. Walden and M. A. Tivey, Near-bottom magnetic surveys of the Coaxial Ridge segment using the Autonomous Benthic Explorer survey vehicle, *RIDGE Events*, 7, 5–9, 1996.
- Yoerger, D.R., R. Collier, and A.M. Bradley, Hydrothermal Vent Plume Discovery and Survey with an Autonomous Underwater Vehicle, *Eos Trans. AGU*, 83(47), Fall Meet. Suppl., Abstract T11C-1261, 2002.

Daniel J. Fornari, Woods Hole Oceanographic Institution, Geology and Geophysics Department, Clark South 172, MS 24, 286 Woods Hole Road, Woods Hole, MA 02543. (dfornari@whoi.edu)

